CHAPTER FOUR

IMPURE CALCAREOUS ROCKS

4.1 INTRODUCTION

In the southern part of the New England Fold Belt, calcareous and impure calcareous sediments occur predominantly within the Tamworth Group, which outcrops in a belt 5-10 km wide to the west of the Peel Fault (Chappell, 1959 and Ellenor, 1975). The only plutons of the New England Batholith to intrude and contact metamorphose these sediments are the Inlet Monzonite and the Moonbi Adamellite (Fig. 4-1).

In the study area, the unmetamorphosed impure calcareous rocks mainly consist of clastic mixtures of calcareous (carbonate rich) and non-calcareous material, with the latter comprising psammitic, pelitic, and volcanic detritus. The bulk composition of rocks of this type is approximated by the K_2O-CaO-MgO-Al_2O_3-SiO_2-CO_2-H_2O system, as reviewed by Kerrick (1974). Although these rocks are referred to here as impure calcareous rocks (after Thompson, P.H., 1973) the synonymous terms 'impure limestones' and 'impure carbonate rocks' are commonly used in the literature (e.g. Kerrick, 1974 and Thompson, 1975b respectively). Other terms used to describe rocks of this type include argillaceous carbonate rocks (Ferry, 1976), micaceous limestones (Hewitt, 1973), calc-mica schists (Thompson, 1975b), calc-schists (Erdmer, 1981), and marly rocks (Winkler, 1976; Hoschek, 1980). However, these terms are considered to be inappropriate for the rocks of this study. The broad classification of Pettijohn (1975), which subdivides detrital limestones into calcirudites, calcarenites, and calcilutites, is used here to identify separate calcareous units. However, other terms (e.g. biomicrite) are also used where appropriate.

Five metamorphic zones have been recognised within the impure calcareous rocks, based on reactions in the K_2O-CaO-MgO-Al_2O_3-SiO_2-CO_2-H_2O system. Metamorphic grade is taken to be directly related to distance from the pluton. The aureole around the Inlet Monzonite is approximately 2 km wide, whereas that around the Moonbi Adamellite extends to at least 3 km.

Calc-silicate reaction bands occur between chemically different blocks within the calcirudites. Garnet skarns occur at the contact between

Figure 4-1: The location of areas at which contact metamorphism of the impure calcareous rocks has been studied. The grid corresponds to that on the Tamworth and Manilla 1:250 000 geological sheets.

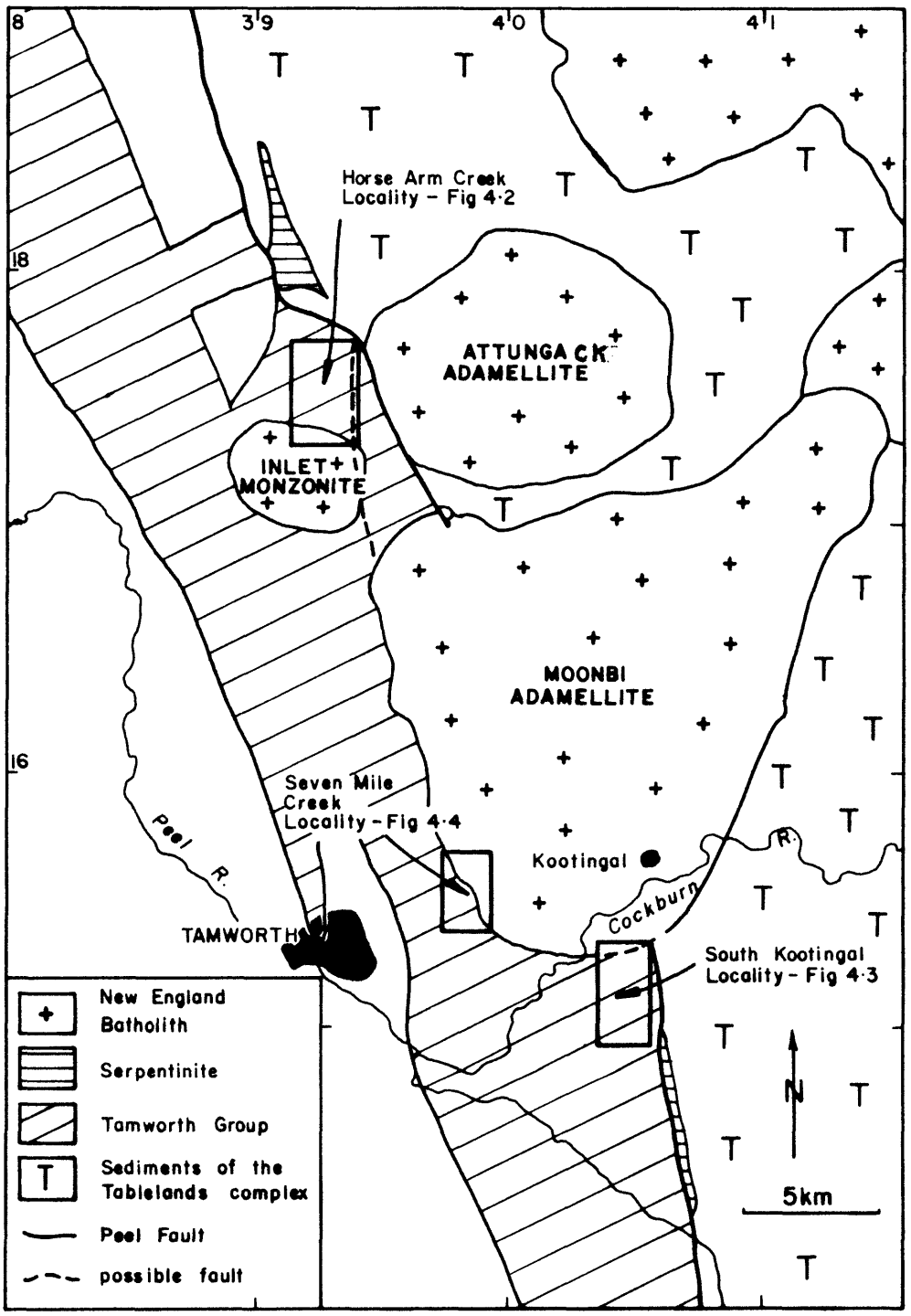
8
3'9
4'0
4'1
18
16
Horse Arm Creek
Locality - Fig 4·2
ATTUNGA CK
ADAMELLITE
INLET
MONZONITE
MOONBI
ADAMELLITE
Seven Mile
Creek
Locality - Fig 4·4
Peel R.
TAMWORTH
Kootingal
Cockburn R.
South Kootingal
Locality - Fig 4·3
N
5km
New England
Batholith
Serpentinite
Tamworth Group
Sediments of the
Tablelands complex
Peel Fault
possible fault

relatively pure limestones and the Inlet Monzonite, produced by metasomatic alteration of the original limestone. These features are not considered further in this chapter, which is not concerned with the effects of metasomatism. The reaction bands are studied in detail in Chapter Five. A map of the skarn locality is shown in Appendix One.

4.2 PETROGRAPHY AND METAMORPHISM OUTSIDE THE AUREOLES

Calcareous rocks of the Tamworth Group remote from the plutons were examined for lithological variation and metamorphic grade before thermal metamorphism. Limestones consisting almost totally of calcite are abundant. These are typically fossiliferous (favosite corals being most prominent). Brecciated limestones, consisting of limestone fragments within a calcite-rich matrix, are also common. The limestone fragments within these breccias are typically outlined by microstylolites containing thin stringers of chlorite and opaques (e.g. sample T65), and these limestones will be referred to as stylolitic limestones in this text. Volcanic calcirudites are commonly associated with the limestones. These are green-coloured rocks consisting of a medium-grained (1-5 mm) mixture of limestone and volcanic fragments within a fine-grained calcareous matrix. These rocks show evidence of very low-grade regional metamorphism, defined by the assemblage prehnite + pumpellyite + chlorite + quartz + calcite (Winkler, 1976). This assemblage has been verified by probe analyses (Table 4.1). Temperatures below 350^{o}C are required for this assemblage (Winkler, 1976, p.188).

Various types of impure calcareous rocks (e.g. impure calcirudites and calcareous litharenites) occur within the Tamworth Group. Contact metamorphism of these rocks has been studied at three specific localities (Section 4.3). The petrography of these rock types outside the aureole at these localities will be described, along with the progressive changes caused by contact metamorphism, in Section 4.4.

4.3 LOCALITIES AND ROCK TYPES INVESTIGATED

The general geology of the three major localities at which contact metamorphism of the impure calcareous rocks has been examined are outlined below.

TABLE 4.1. Microprobe analyses of prehnite, pumpellyite and chlorite from sample T68 (outside the aureole)

	Prehnite		Pumpellyite		Chlorite	
SiO_2	43.69	43.04	35.09	34.43	26.55	27.97
Al_2O_3	20.18	23.69	16.22	16.70	17.69	15.06
Fe_2O_3*	-	-	14.14	12.38	-	-
FeO	3.95	0.41	5.37	5.44	27.58	26.96
MnO	-	-	0.12	-	0.53	0.51
MgO	-	-	0.36	0.38	14.27	14.78
CaO	25.47	27.05	22.00	21.90	0.29	0.18
Na_2O	0.11	-	0.14	-	-	0.14
Total	93.40	94.19	93.44	91.33	86.91	85.60
Structural formulae†						
Si	6.251	6.020	11.968	11.962	5.742	6.123
Al^{IV}	-	-	0.032	0.038	2.258	1.877
Al^{VI}	3.406	3.908	6.494	6.806	2.254	2.012
Fe^{3+}	-	-	3.631	3.239	-	-
$Fe2^{+}$	0.473	0.048	1.532	1.610	4.988	4.936
Mn	-	-	0.035	-	0.097	0.095
Mg	-	-	0.183	0.197	4.599	4.822
Ca	3.905	4.054	8.040	8.153	0.067	0.042
Na	0.031	-	0.093	-	-	0.059
Total Cations	14.066	14.030	32.008	32.005	20.006	19.965
$Mg/Mg+Fe^{2+}$			0.107	0.109	0.480	0.494
$Al^{VI}/Al^{VI}+Fe^{3+}$			0.641	0.678		

* Fe_2O_3 calculated on the basis of 32 cations

† Prehnite based on 22 oxygens
Pumpellyite based on 49 oxygens
Chlorite based on 28 oxygens

4.3.1 Horse Arm Creek

A detailed study has been made of the calcareous units north of the Inlet Monzonite at Horse Arm Creek (Fig. 4-2), where two major limestone horizons are interbedded with psammitic and pelitic beds in a N-S striking sequence. These limestones are very variable both across and along strike. Rock types within the western limestone horizon comprise massive limestones, limestone breccias and conglomerates (impure calcirudities), and impure calcarenites composed of arenaceous grains of calcite, quartz, feldspar, and lithic fragments. Relict fossil outlines (predominantly of corals) remain in the massive limestones, even at high grade. The eastern limestone horizon is less variable, consisting mainly of massive and brecciated near-pure limestones. However, in parts, this unit is interbedded with volcanic and pelitic material. Although the limestones in this unit consist almost entirely of calcite, they typically possess fine stringers of non-carbonate material. These stringers are believed to be concentrations along microstylolites, and these limestones are equivalent to the stylolitic limestones described in Section 4.2. Between the eastern and western limestone horizons, some beds within the psammitic rocks contain a significant carbonate component. A distinct unit of calcareous feldspathic litharenite has been mapped below the eastern limestone horizon (Fig. 4-2). This unit proved to be valuable in defining the metamorphic zones within the aureole. For convenience, the shorter term 'calcareous litharenite' will be used to refer to this rock type.

The northern part of the Horse Arm Creek locality lies near the western contact of the Attunga Creek Adamellite (Fig. 4-1). Although biotite hornfelses are developed at the northern contact of the Attunga Creek Adamellite, the sediments at the Horse Arm Creek locality show no thermal effects related to this intrusion.

In the northern part of Fig. 4-2, granitic scree shed from the Attunga Creek Adamellite to the east obscures the contact of this pluton. Consequently, the relationship between the Peel Fault and the Attunga Creek Adamellite is uncertain (Fig. 4-1). Further knowledge of this relationship is required to understand the lack of thermal effects produced by the Attunga Creek Adamellite within the sediments of the Tamworth Group (west of the Peel Fault).

Figure 4-2: Geological and sample locality map for the Horse Arm Creek locality. The grid corresponds to that on the Attunga 1:25 000 topographic sheet.

Underlined sample locality numbers refer to numbers prefixed by C (e.g. 129 refers to C129). All other sample locality numbers except 371 and 372 refer to numbers prefixed by T (e.g. 85 refers to T85).

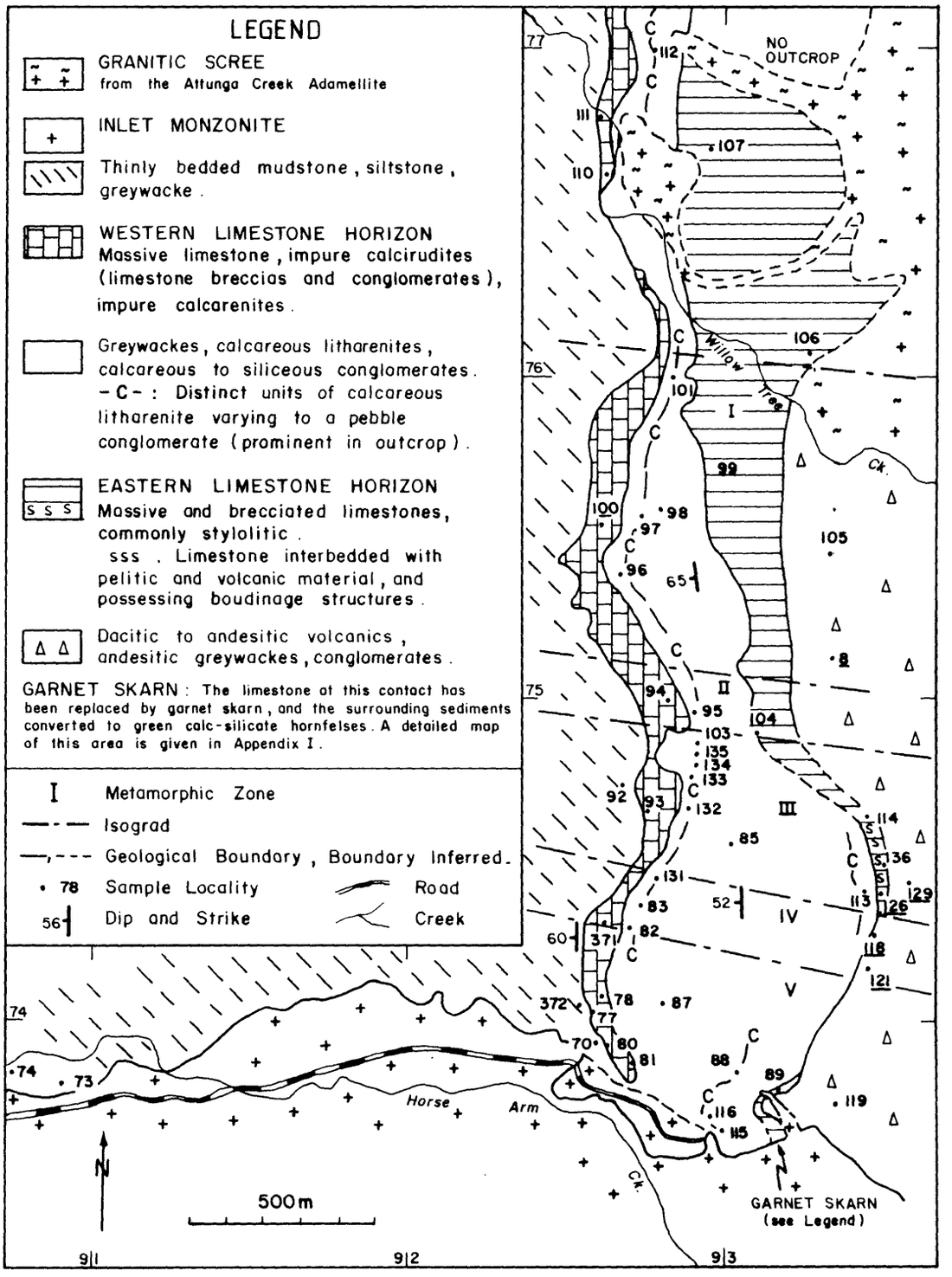
LEGEND
GRANITIC SCREE
from the Attunga Creek Adamellite
INLET MONZONITE
Thinly bedded mudstone, siltstone, greywacke.
WESTERN LIMESTONE HORIZON
Massive limestone, impure calcirudites (limestone breccias and conglomerates), impure calcarenites.
Greywackes, calcareous litharenites, calcareous to siliceous conglomerates.
-C-: Distinct units of calcareous litharenite varying to a pebble conglomerate (prominent in outcrop).
EASTERN LIMESTONE HORIZON
Massive and brecciated limestones, commonly stylolitic.
sss. Limestone interbedded with pelitic and volcanic material, and possessing boudinage structures.
Dacitic to andesitic volcanics, andesitic greywackes, conglomerates.
GARNET SKARN: The limestone at this contact has been replaced by garnet skarn, and the surrounding sediments converted to green calc-silicate hornfelses. A detailed map of this area is given in Appendix I.
I Metamorphic Zone
Isograd
Geological Boundary, Boundary Inferred.
78 Sample Locality
Road
56 Dip and Strike
Creek
NO OUTCROP
Willow Tree Ck.
Horse Arm
Ck.
GARNET SKARN (see Legend)
N
500m
9|1
9|2
9|3

4.3.2 South Kootingal

In the region south of Kootingal (Figs. 4-1 and 4-3), several limestone units, ranging from near-pure calcirudites to calcareous rudites, occur within the southern aureole of the Moonbi Adamellite. These limestones are associated with volcanic breccias, and many of the calcareous rudites appear to be a mixture of this volcanic material with the near-pure limestones.

4.3.3 Seven Mile Creek

At the western contact of the Moonbi Adamellite (Seven Mile Creek locality) an anticlinal structure has been mapped within limestones, shales, and volcanic litharenites (Fig. 4-4). The limestone varies from an impure biomicrite, containing shell fragments within a marly matrix, to a coarser-grained impure calcirudite.

4.4 PETROGRAPHY OF THE CONTACT METAMORPHOSED ROCKS

4.4.1 Introduction

Five metamorphic zones have been mapped within the impure calcareous rocks on the basis of the appearance and disappearance of characteristic assemblages. These are:

I) Biotite Zone
II) Clinopyroxene Zone
III) Garnet Zone
IV) Wollastonite Zone
V) Wollastonite + Plagioclase Zone.

These zones were primarily established in the calcareous litharenites in the northern aureole of the Inlet Monzonite. They were further substantiated by considering matrix assemblages in the impure calcirudites from all three localities. Detailed description of the zones in these two rock types is given in Sections 4.4.2 and 4.4.3. This is followed by brief descriptions of the contact metamorphism of the impure biomicrites and stylolitic limestones.

Figure 4-3: Geological and sample locality map for the South Kootingal locality. The grid corresponds to that on the Moonbi 1:25 000 topographic sheet.

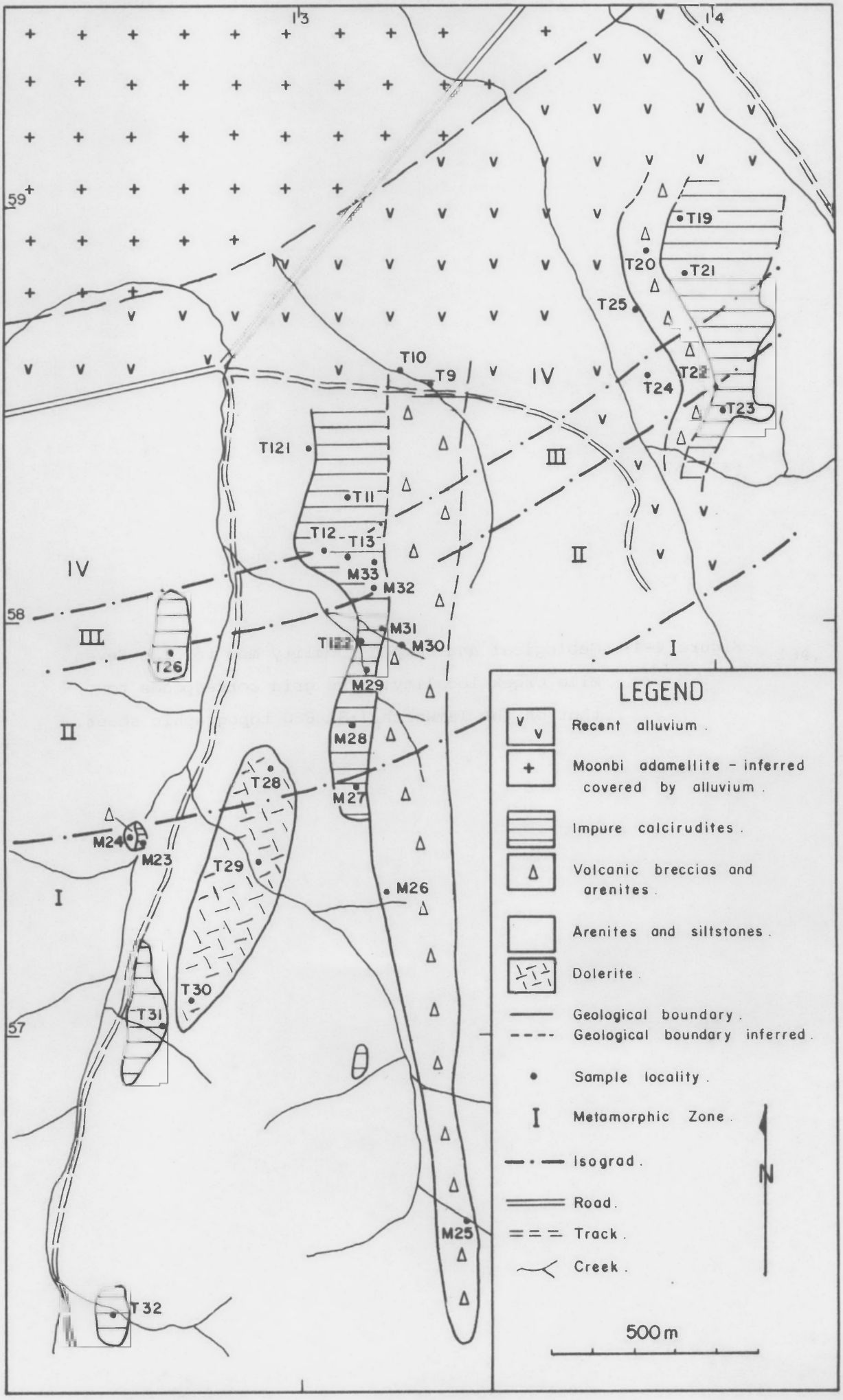
13
14
59
58
57
T19
T20
T21
T25
T22
T24
T23
T10
T9
T121
T11
T12
T13
M33
M32
M31
T122
M30
M29
M28
M27
T28
M24
M23
T29
M26
T30
T31
T32
M25
T26
I
II
III
IV
LEGEND
Recent alluvium.
Moonbi adamellite - inferred covered by alluvium.
Impure calcirudites.
Volcanic breccias and arenites.
Arenites and siltstones.
Dolerite.
Geological boundary.
Geological boundary inferred.
Sample locality.
Metamorphic Zone.
Isograd.
Road.
Track.
Creek.
N
500 m

Figure 4-4: Geological and sample locality map for the Seven Mile Creek locality. The grid corresponds to that on the Tamworth 1:31 680 topographic sheet.

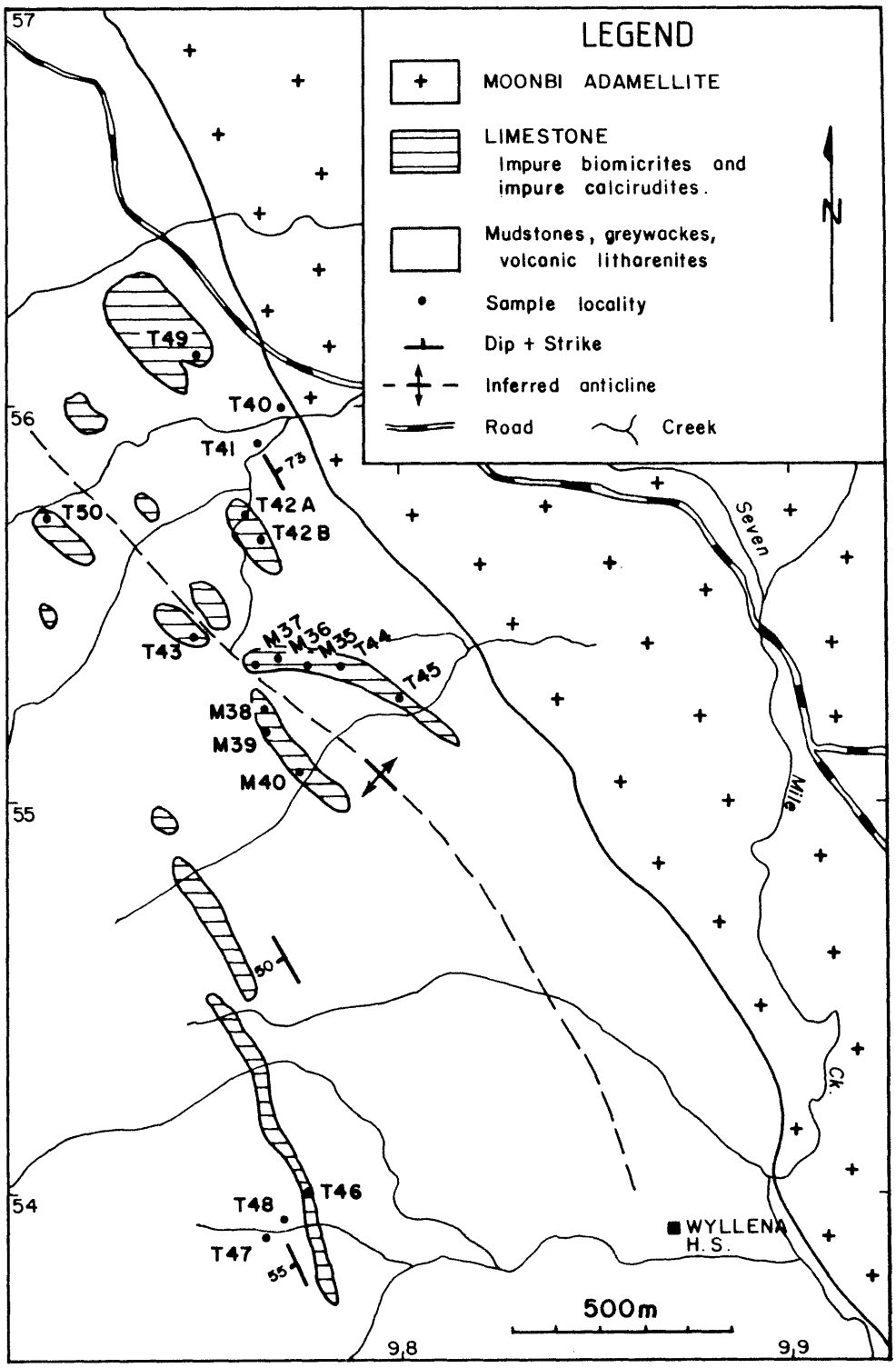
LEGEND
MOONBI ADAMELLITE
LIMESTONE
Impure biomicrites and impure calcirudites.
Mudstones, greywackes, volcanic litharenites
Sample locality
Dip + Strike
Inferred anticline
Road
Creek
N
57
56
55
54
T49
T40
T41
73
T42A
T42B
T50
T43
M37
M36
M35
T44
T45
M38
M39
M40
50
T48
T46
T47
55
Seven Mile Ck.
WYLLENA H.S.
500m
9,8
9,9

4.4.2 Calcareous Litharenites

Although the following discussion is based primarily on the calcareous litharenites at the Horse Arm Creek locality (Fig. 4-2), the impure calcarenites from the western limestone horizon at the same locality were also considered. Distances from the contact of the Inlet Monzonite are given in brackets for each zone.

Outside the Aureole

Outside the aureole at the Horse Arm Creek locality, the calcareous litharenites consist of an accumulation of various crystal and lithic fragments. The lithic fragments comprise calcareous, volcanic, pelitic, and psammitic material, while the crystal fragments consist of quartz, calcite, K-feldspar and plagioclase (approx. An 50). Interstitial to these fragments is a mixture of chlorite, calcite, and fine-grained felsic material. This texture is depicted in Plate 4-1A. Saussuritisation of plagioclase is common in these rocks outside the aureole; the plagioclase is altered to a fine-grained mixture of calcite, epidote and sericite. Epidote also occurs within the matrix. This epidote is considered here to be a product of regional metamorphism, though it may mark the very outer effects of thermal metamorphism.

Biotite Zone (2 km - 1100 m)

The outer limit of contact metamorphism is denoted by the appearance of fine-grained green biotite. Epidote is also present, and these phases commonly coexist within patches of chlorite (Plate 4-1B). Biotite also coexists with a dark-green calcic amphibole, again typically within fibrous clusters of chlorite (Plate 4-1C). However, epidote and amphibole are not found together.

Staining with sodium cobaltinitrite has shown that K-feldspar is lost at the biotite isograd. This K-feldspar provides an obvious source of potassium for the formation of green biotite. Saussuritisation of plagioclase is no longer common. The overall texture of the rock remains similar to that outside the aureole, with lithic and crystal fragments predominant.

Clinopyroxene Zone (1100 m - 950 m)

This zone is characterised by the incoming of clinopyroxene +

Plate 4-1: Textures in calcareous litharenites from the Horse Arm Creek locality (at grades below the clinopyroxene isograd).
Photographs taken under plane-polarized light

A: Outside the Aureole (Sample T112).
Clastic texture of crystal and lithic fragments. The crystal fragments consist of quartz (clear), feldspar (brownish alteration - saussuritisation) and calcite (showing twin lamellae). Interstitial chlorite (c) is shown bent around the fragments. Width of the photograph covers 3.60 mm.

B: Biotite Zone (Sample T101A).
Epidote (e) and biotite (b) coexist within an interstitial patch of chlorite (c). Width of the photograph covers 0.90 mm.

C: Biotite Zone (Sample T97).
Calcic-amphibole (a) and biotite (b) coexist within an interstitial patch of chlorite (c). Width of the photograph covers 0.90 mm.

A

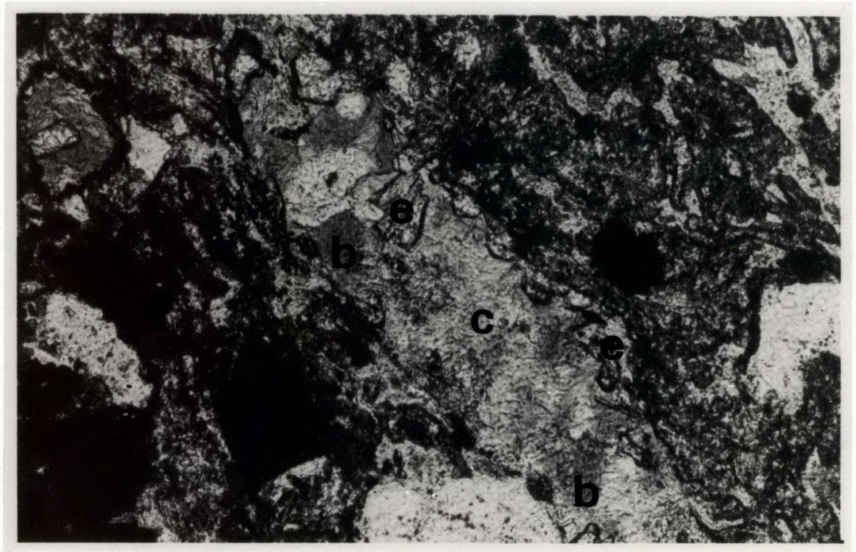

B

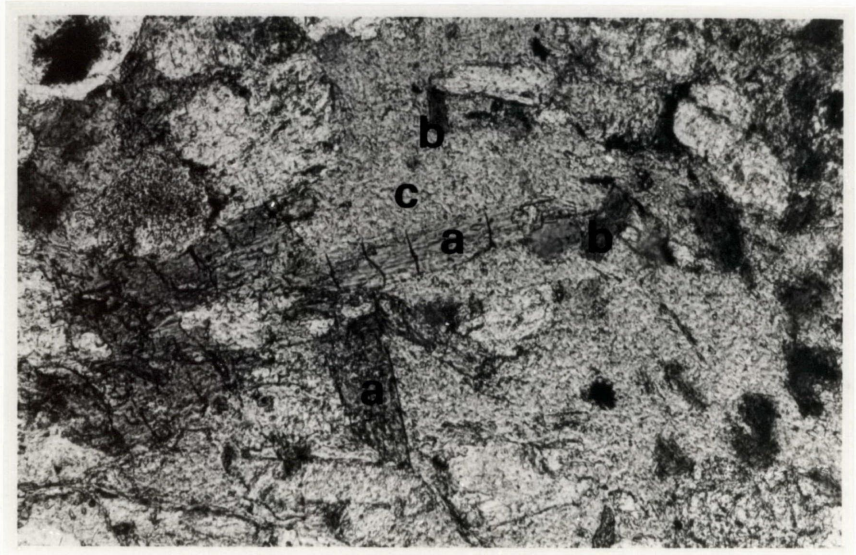

C

K-feldspar and the immediate loss of biotite. The rock continues to show little change in texture, except that the fine-grained matrix is replaced by a semi-granoblastic aggregate of clinopyroxene, K-feldspar, and commonly epidote (Plate 4-2A). The crystal fragments continue to consist of calcite, quartz, and plagioclase, with the plagioclase showing no sign of alteration to epidote. A fine-grained brownish material, probably sphene, is common.

A distinct decrease in chlorite, and loss of the assemblage chlorite + calcite, coincides with the incoming of clinopyroxene. Where large patches of chlorite remain, they are characteristically overgrown by coarse idioblastic epidote and amphibole. Therefore, it appears that chlorite + calcite, present within the biotite zone, is unstable with respect to epidote + amphibole in the clinopyroxene zone (discussed further in Section 4.6).

Textural evidence also demonstrates the unstable coexistence of calcic amphibole and calcite, for amphibole adjacent to calcite-rich (limestone) fragments has been replaced by clinopyroxene. Amphibole is therefore uncommon in the clinopyroxene zone, being restricted to chlorite-rich patches, and to basic lithic fragments containing amphibole + plagioclase ± epidote (i.e. where calcite is absent). Similarly, where these basic fragments are in contact with limestone fragments, the former are typically altered to clinopyroxene + plagioclase-bearing assemblages at their edges.

Garnet Zone (950 m - 650 m)

The outer boundary of this zone is marked by an immediate abundance of garnet throughout the rocks. The incoming of garnet is easily recognised in the field by its red-brown colour in hand specimen. In thin section, the garnet forms as relatively coarse grains up to 2 mm across, within a much finer-grained assemblage of clinopyroxene, K-feldspar, plagioclase and quartz. A major decrease is noted in the number of opaque grains, with the garnet zone being almost opaque-free. Although amphibole is not a member of the above assemblage, it persists with plagioclase in the basic lithic fragments. Fine-grained sphene is quite distinct and commonly occurs around yellow grains of rutile.

The matrix is totally reconstituted in the garnet zone, with the

Plate 4-2: Textures in calcareous litharenites from the Horse Arm Creek locality (at grades above the clinopyroxene isograd).

Photographs taken under plane-polarized light.

A: Clinopyroxene Zone (Sample T95A).
Granular clinopyroxene (black in the photograph) and K-feldspar (white amongst clinopyroxene) occur between crystal fragments of plagioclase (grey-clouded appearance) and quartz (two large grains left of centre-q). Width of photograph covers 3.60 mm.

B: Wollastonite Zone (Sample T131B).
Wollastonite (w) replaces previous quartz fragments (cf. photograph 4-2A). The wollastonite has a columnar to fibrous texture. Other fragments are predominantly relict plagioclase. The dark assemblage between the fragments consists mainly of garnet, clinopyroxene and feldspar. Width of photograph covers 3.60 mm.

C: Wollastonite + Plagioclase Zone (Sample T87).
Granoblastic-polygonal aggregate of wollastonite (w), plagioclase (p), garnet (g) and clinopyroxene (c). Width of photograph covers 0.90 mm.

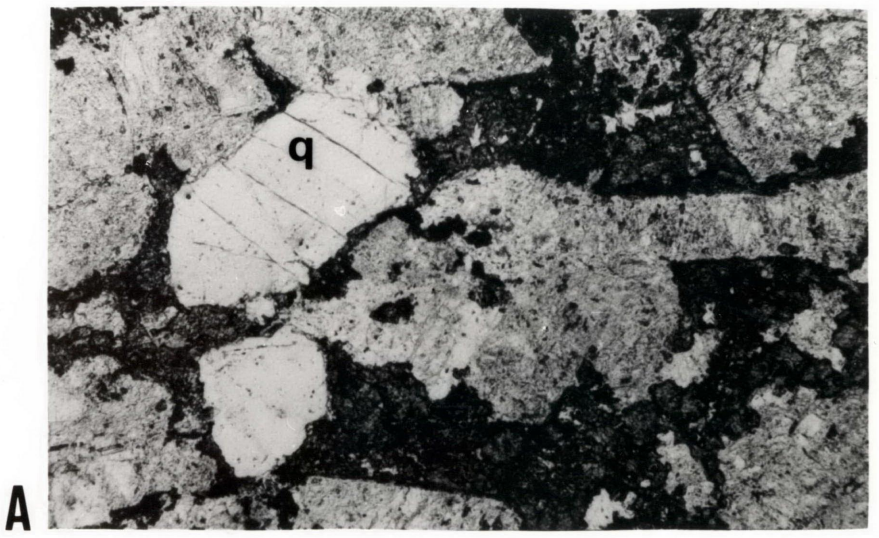

A

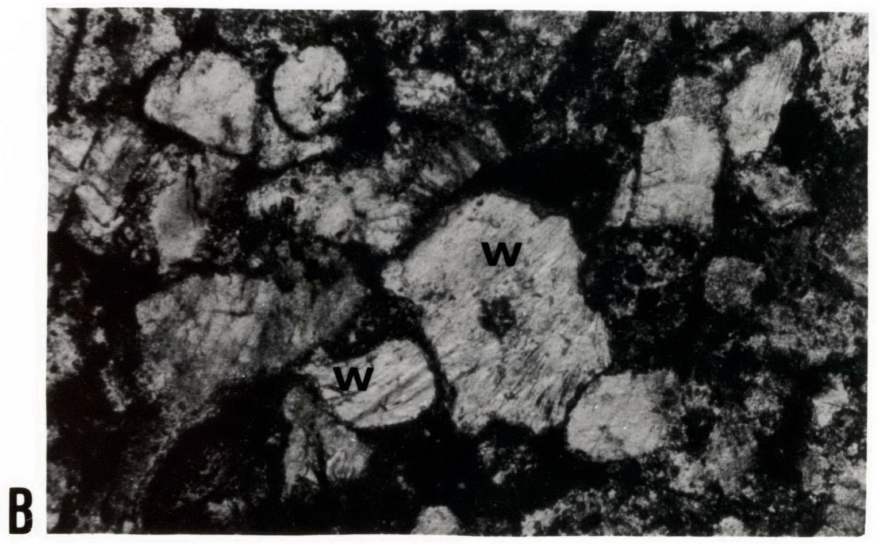

B

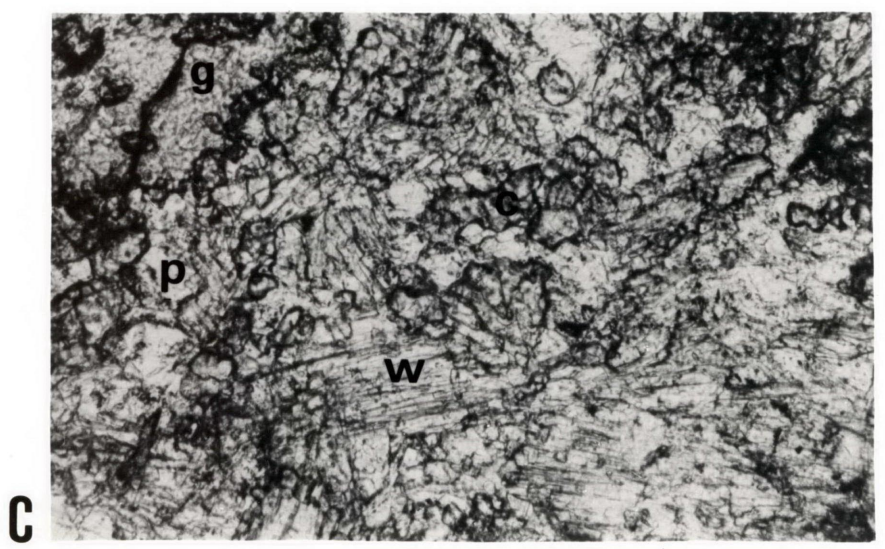

C

above assemblage forming a well developed granoblastic-polygonal texture. Lithic fragments have been internally modified to fine-grained granoblastic-polygonal assemblages. However, their outlines are still clearly defined and readily identifiable in thin section. The crystal fragments appear to be unaffected and remain as relict grains, conspicuous amongst the otherwise totally metamorphic texture.

Calcite crystal fragments are lost at the garnet isograd. Therefore, crystal fragments in the garnet zone consist only of plagioclase and quartz, with plagioclase the more abundant. However, calcite was not totally lost at this boundary, for it persists as patches completely enclosed within coarse garnet, and as small grains within the matrix. Stable contacts between calcite and quartz have been found. However, the assemblage calcite + quartz + plagioclase was not recognised within the garnet zone. Epidote (? retrograde) is still evident in the outer part of the garnet zone, where it is commonly associated with garnet, and often enclosed by it.

Wollastonite Zone (650 m - 350 m)

Wollastonite first occurs within the fine-grained calcareous rocks as discrete fibrous clusters. It directly replaces previous crystal fragments of quartz, the outlines of which are still apparent (Plate 4-2B). Similarly, wollastonite is enclosed within garnet grains, in place of the previously enclosed calcite (described above). Hence, the breakdown of quartz + calcite to wollastonite is believed to have occurred. The matrix of the original rock has been metamorphosed to the assemblage garnet + clinopyroxene + K-feldspar + plagioclase + quartz (?) + sphene possessing a granoblastic-polygonal texture. Wollastonite does not form part of this granoblastic assemblage, but is restricted to the occurrences described above. Therefore, although plagioclase and wollastonite may occur within the same thin section, there is no textural evidence to suggest that wollastonite + plagioclase is stable within this zone. Relict euhedral plagioclase grains continue to be conspicuous amongst the metamorphic assemblage. Although lithic fragments are still discernible, grain growth within them has made their recognition difficult in thin section.

Wollastonite + Plagioclase Zone (350 m - contact)

This zone is marked by the occurrence of wollastonite in textural

equilibrium with plagioclase. The wollastonite no longer occurs as discrete clusters (as in the wollastonite zone), but as part of the granoblastic-polygonal texture (Plate 4-2C), which in this zone is developed almost throughout the entire rock. The metamorphic assemblage consists of wollastonite + garnet + clinopyroxene + K-feldspar + plagioclase + sphene. Quartz is not apparent within this zone. Relict grains of plagioclase remain in the rocks, but their abundance is significantly reduced. Coarsening of the overall assemblage makes the relict plagioclase less conspicuous in this zone than that at lower grades. The relict plagioclase is typically jagged in outline resulting from the formation of metamorphic plagioclase grains at its edges. Probe analyses show that within the same thin section the relict grains of plagioclase are more anorthitic than those in textural equilibrium with the metamorphic assemblage (see Section 4.5.6).

4.4.3 Impure Calcirudites

This section describes the progressive contact metamorphism of the matrix material in the impure calcirudites. These rocks are typically of two types. One consists predominantly of limestone fragments within a marly matrix, whereas the other comprises pebbles and boulders of calcareous and non-calcareous material within a fine-grained matrix of lithic and crystal fragments. The contact metamorphism of these two types can be considered together. Because the impure calcirudites were examined at three different localities, it is convenient to discuss their contact metamorphism at each locality separately. However, a brief comment on their petrography outside the aureole is given first.

Outside the Aureole

The impure calcirudites with a marly matrix were not found outside the aureole. The second type, containing an arenaceous matrix, has been found outside the northern aureole of the Inlet Monzonite, and their description is applicable to all three localities. These impure calcirudites are composed of very coarse-grained lithic fragments, mostly of limestone (calcite), but also of pelitic, psammitic and volcanic material. The matrix in these rocks resembles the calcareous litharenites in appearance. It consists of a mixture of fine-grained lithic fragments, similar in compositional range to the coarser-grained fragments, and

crystal fragments of quartz, calcite, K-feldspar and plagioclase. Chlorite is interstitially interwoven around the fragments, while sericite, although not ubiquitous, is commonly associated with the chlorite.

Horse Arm Creek (Fig. 4-2)

Impure calcirudites occur mainly within the western limestone horizon. Only an incomplete sequence of metamorphic zones could be identified because of variation along the unit and the abundance of pure limestone within it. However, the sequence of metamorphic changes detected is broadly consistent with that found in the calcareous litharenites. No impure calcirudite was found between the outer limit of the aureole and 1 km from the contact of the Inlet Monzonite. At 1 km from the pluton, clinopyroxene occurs throughout the matrix and crystal fragments of calcite, quartz and feldspar are prevalent. By 350m from the contact the matrix is strongly retextured, with only relict crystals of plagioclase remaining within a granoblastic-polygonal matrix of wollastonite + garnet + clinopyroxene + plagioclase + K-feldspar. The assemblage is unchanged at 100m from the contact, but the granoblastic-polygonal texture is further developed.

South Kootingal (Fig. 4-3)

The impure calcirudites in this area afford the best sequence of metamorphic zones obtained from this rock type, but again the lithological variation and lack of continuous outcrop hindered locating zone boundaries. Also, the contact of the Moonbi Adamellite in this region is covered by recent alluvium, so that distances from the contact were estimated from an inferred pluton border. Therefore, locating zone boundaries with respect to the pluton contact is only approximate, especially for the inner zones. The sequence of zones found, and proposed distances from the contact are

I) Biotite Zone (>2.5 km - 1250 m)
II) Clinopyroxene Zone (1250 m - 850 m)
III) Garnet Zone (850 m - approx. 700 m)
IV) Wollastonite Zone (approx. 700 m - contact).

The zones are defined on the same criteria as in the calcareous litharenites, and the sequence of zones is identical to that described in those rocks. Previously described textures from within the finer rocks are also present

within the matrixes of the calcirudites. A wollastonite + plagioclase zone could not be identified within this aureole, because sediments close to the contact were too poor in Ca to form wollastonite-bearing assemblages. Location of the zones around the plutons is largely dependent on size and composition of the pluton involved (Chapter One, 1.6,2). However, it is noteworthy that, although the aureole around the Moonbi Adamellite is wider than that around the Inlet Monzonite, the garnet zone in the impure calcirudites at this locality is thinner than that described in the calcareous litharenites at the Horse Arm Creek locality (discussed in Section 4.7.3).

Seven Mile Creek (Fig. 4-4)

The rudaceous rocks in this area are also very variable in composition. The impure calcirudites were all found within 250 metres of the contact and contain metamorphic assemblages rich in clinopyroxenes, garnet and wollastonite. Coarse-grained assemblages in these rocks commonly consist of only one or two phases. For example, assemblages of idioblastic garnet and clinopyroxene are common, as are assemblages of coarse-grained interlocking garnet and wollastonite. These variations appear to reflect not only differences within the original rock, but also the probable occurrence of extensive diffusion during metamorphism (described in Chapter Five).

4.4.4 Impure Biomicrites

The best examples of these rocks are in the Seven Mile Creek locality (Fig. 4-4). Sample T46B (at 1 km from the Moonbi Adamellite) represents the lowest grade of metamorphism found within the impure biomicrites. It has both rounded and angular fragments of coarse-grained calcite, which are believed to be recrystallised fossiliferous material. The remainder of the rock consists of calcite, quartz and feldspar crystal fragments within a fine-grained matrix composed of calcite, an unidentified felsic component, and biotite. At 700m from the contact, little change has occurred except that small grains of clinopyroxene have formed at the edges of calcite fragments. However, at 500m from the contact, wollastonite occurs at the edges of the calcite fragments, and the matrix has altered to an assemblage of clinopyroxene + quartz + feldspar, plus minor opaques and sphene. The mineral assemblage does not change with further increase in grade, but by 200m from the contact the matrix has

developed a granoblastic-polygonal texture, and wollastonite formation has intensified at the edges of the calcite fragments. Calcite remaining in the centre of the fragments has developed a coarse-grained granoblastic-polygonal texture.

A calcareous unit containing large pelitic fragments is associated with the biomicrites, and near the pluton contact, although the centres of the pelitic fragments have biotite-rich assemblages, the edges of the fragments (contacting the calcareous matrix) have been converted to clinopyroxene + feldspar + quartz. Clearly the major changes within these rock units has been the breakdown of biotite + calcite to clinopyroxene at about 700m from the contact, and the formation of wollastonite (without previous garnet formation) from calcite + quartz at approximately 500m from the contact. These changes will be discussed in relation to the CO_2 content of these rocks in Section 4.7.4.

4.4.5 Stylolitic Limestones

These limestones are composed predominantly of calcite, with only minor non-carbonate impurities. The best examples of this rock type are associated with the massive and interbedded limestones of the eastern limestone horizon north of the Inlet Monzonite. Sample T107, from outside the aureole at this locality, is a calcite-rich rock containing thin stringers of chlorite, Fe oxide, Fe sulphide and minor sericite.

At 1 km from the contact, the limestone fragments and interstitial material are still distinguishable. The non-carbonate component, however, now consists of fine flakes of phlogopite associated with Fe oxide and Fe sulphide. At the contact, the stylolitic limestones have been metamorphosed to impure marbles, and practically all features of the original rock have been obliterated. These marbles contain round grains of forsterite (Mg/Mg+Fe = 0.974), Fe oxide, Fe sulphide, and lesser amounts of spinel (Mg/Mg+Fe = 0.940), within a mosaic of coarse-grained calcite.

Insufficient samples of these rocks were available throughout the aureole to define metamorphic zones and appropriate reactions. However, their mineralogy is clearly distinct from that of previously described rock types. This variation in mineralogy with rock type is briefly discussed in Section 4.6.3.

4.5 MINERAL CHEMISTRY

4.5.1 Introduction

The majority of impure calcareous rocks studied here can be defined by the system K_2O-CaO-MgO-Al_2O_3-SiO_2-CO_2-H_2O. However, variable solid solution in the phases will alter the metamorphic conditions at which reactions occur within this system (e.g. Ghent and De Vries, 1972; Kerrick *et al.*, 1973; Kerrick, 1974, p.749; Thompson, 1975b; Kerrick, 1977). The phases have been analysed to allow for these effects; of prime concern were the substitution of Na_2O for CaO, FeO for MgO, and Fe_2O_3 for Al_2O_3. Attempts have been made to identify any variations in mineral chemistry related to increasing grade, though variations in whole-rock chemistry have made these difficult to recognise. The distribution of elements between phases will be discussed where appropriate.

4.5.2 Low-Grade Ferromagnesians - Chlorite, Biotite, Amphibole, Clinopyroxene

Selected analyses of ferromagnesian phases from the outer part of the aureole are given in Table 4.2. The minerals vary in composition from sample to sample, apparently related to variations in whole-rock chemistry. No systematic trends with increasing grade could be substantiated. By comparing analyses of coexisting phases (as denoted in Table 4.2), the relative Mg/Mg+Fe ratios (X_{Mg}) of the ferromagnesian minerals can be given as

$$X_{Mg}^{Pyroxene} > X_{Mg}^{Amphibole} > X_{Mg}^{Chlorite} > X_{Mg}^{Biotite} .$$

Some variations in mineral chemistry are a consequence of differences in paragenesis, unrelated to differences in metamorphic grade. For example, amphibole grains occurring with epidote (e.g. T95 A # 2) are more Mg-rich than those associated with either clinopyroxene (e.g. T26) or biotite (e.g. T97) (Table 4.2). This is because of the inability of epidote to take Mg into its structure. Biotite associated with epidote shows a similar effect (compare the biotite analyses of samples T31 and T97 in Table 4.2).

Phlogopite (Mg/Mg+Fe = 0.875-0.925)-bearing stylolitic limestones (e.g. sample T104) have been described in Section 4.4.5. The high Mg/Mg+Fe ratios of these biotites are unlikely to be solely related to

TABLE 4.2. Microprobe analyses of low-grade biotite, chlorite, amphibole and clinopyroxene in impure calcareous rocks

	Biotite		Chlorite			Amphibole			Clinopyroxene	
Associated Minerals*	Chl Amph	Chl Ep	Bi Amph	Bi Ep	Cpx	Chl Bi	Cpx	Chl Ep	Amph	Chl
Sample No.	T97	T31	T97	T31	T95A-1	T97	T26-2	T95A-2	T26-2	T95A-1
SiO_2	36.20	37.89	25.44	28.48	23.90	46.84	46.95	47.60	51.98	49.84
TiO_2	1.17	1.14	-	-	-	0.15	0.30	-	-	-
Al_2O_3	16.49	17.31	21.57	19.69	18.87	8.31	7.49	7.76	1.48	0.53
Fe_2O_3**	-	-	-	-	-	6.92	4.24	4.83	1.79	1.24
FeO	18.07	13.40	22.42	16.34	36.01	11.24	12.60	8.21	9.57	20.46
MnO	-	-	0.20	-	0.21	0.20	-	0.20	-	0.14
MgO	12.90	15.71	17.96	23.01	7.38	12.17	12.52	15.37	11.43	4.63
CaO	-	0.23	-	0.10	0.22	11.79	12.67	12.72	24.40	23.60
Na_2O	-	-	0.39	0.29	0.29	0.97	0.85	1.36	0.21	0.16
K_2O	10.15	9.66	-	-	-	0.08	0.61	0.53	-	-
Total	94.98	95.34	87.98	87.90	86.88	98.67	98.22	98.58	100.86	100.60
Structural formulae†										
Si	5.526	5.590	5.273	5.690	5.442	6.830	6.906	6.860	1.949	1.973
Al^{IV}	2.475	2.410	2.727	2.310	2.558	1.170	1.094	1.140	0.051	0.025
Al^{VI}	0.494	0.601	2.546	2.326	2.509	0.259	0.206	0.179	0.015	-
Ti	0.134	0.127	-	-	-	0.016	0.033	-	-	-
Fe^{3+}	-	-	-	-	-	0.760	0.469	0.524	0.051	0.037
Fe^{2+}	2.307	1.653	3.886	2.732	6.857	1.371	1.550	0.989	0.300	0.677
Mn	-	-	0.035	-	0.041	0.025	-	0.024	-	0.005
Mg	2.935	3.454	5.548	6.856	2.504	2.645	2.745	3.301	0.639	0.273
Ca	-	0.036	-	0.022	0.054	1.842	1.977	1.964	0.980	1.001
Na	-	-	0.157	0.111	0.128	0.274	0.242	0.380	0.015	0.012
K	1.977	1.818	-	-	-	0.015	0.114	0.097	-	-
Total cations	15.848	15.689	20.172	20.047	20.093	15.207	15.356	15.458	4.000	4.003
$Mg/Mg+Fe^{2+}$	0.560	0.592	0.588	0.715	0.268	0.659	0.639	0.769	0.681	0.287

** Fe_2O_3 calculated by method of Papike *et al.* (1974).

† Biotite based on 22 oxygens, chlorite - 28 oxygens, amphibole - 23 oxygens, clinopyroxene - 6 oxygens.

* Chl = chlorite, amph = amphibole, ep = epidote, bi = biotite, cpx = clinopyroxene

T95A, T97 are calcareous litharenites from the Horse Arm Creek locality.

T26, T31 are impure calcirudites from the South Kootingal locality.

host-rock composition, because abundant Fe oxides and Fe sulphides occur in these rocks. More probably, it is the biotite's coexistence with these Fe-rich opaques, rather than with epidote or amphibole (as in the calcareous litharenites and impure calcirudites), which has caused Mg to be enriched in the biotite.

4.5.3 Garnet

Garnet compositions from the calcareous litharenites, at various distances from the contact, are shown in Table 4.3. The typical garnet composition in these rocks is around andradite 63-grossular 37, with minor amounts of almandine, spessartine and pyrope. Their $Al/Al+Fe^{3+}$ values vary from 0.35 to 0.45, but no systematic change is evident with increasing grade. This garnet is red-brown to brown in colour. It is typically isotropic, but can show slight birefringence. Differences in garnet composition occur between the rock types. Those in the impure calcirudites are richer in grossular (higher Al/Al+Fe ratios) than those in the calcareous litharenites (Table 4.3). These more grossular-rich garnets are paler in colour (often colourless), and typically show a grey-blue interference colour and optical zoning. The chemistry of the garnets with regard to their optical features will be discussed further in Chapter Five.

4.5.4 Clinopyroxene (with garnet)

Analyses of clinopyroxenes associated with garnet are given in Table 4.4. Six analyses from the calcareous feldspathic litharenites at various distances from the contact are shown. Comparison of these with clinopyroxene analyses in Table 4.2 shows no obvious change in clinopyroxene composition associated with the incoming of garnet. Similarly, although there is a significant range in the clinopyroxene Mg/Mg+Fe ratio (0.217 → 0.614), no systematic change with increasing grade is evident. A positive correlation exists between the Mg/Mg+Fe ratio of the clinopyroxene and the $Al/Al+Fe^{3+}$ ratio of the garnet, in these analyses, and this reflects a variation in the Fe content of the rocks.

As with the garnets, clinopyroxene compositions vary between rock types. Although there is considerable overlap, the coarser-grained sediments tend to give a range of Mg/Mg+Fe values higher than that in the calcareous litharenites.

TABLE 4.3. Microprobe analyses of garnets in impure calcareous rocks

	Calcareous Litharenites							Impure Calcirudites			
Sample No.	T103-1	T103-2	T132A-2	T83B	T87	T80	T81B	371-B	371-1	T11A	T12
Distance (m)*	950	950	750	450	250	100	75	350	350	600	700
SiO_2	36.29	36.53	36.88	36.11	36.44	36.72	36.94	38.34	38.45	39.00	38.57
TiO_2	1.60	1.55	0.63	1.06	0.87	1.30	1.18	1.14	0.46	0.11	0.26
Al_2O_3	7.16	9.71	9.08	8.15	7.59	9.50	7.21	15.96	18.22	19.82	18.08
Fe_2O_3**	19.45	17.33	19.30	20.05	20.82	17.29	20.71	9.31	6.43	5.17	6.57
FeO	1.36	0.62	-	0.89	-	0.55	0.57	0.55	-	0.16	-
MnO	0.53	0.44	-	-	0.50	-	0.16	-	-	0.15	-
MgO	0.12	-	-	-	-	-	0.11	-	0.10	-	-
CaO	33.34	34.34	35.21	33.76	34.30	34.75	35.00	36.15	36.86	36.23	36.77
Total	99.85	100.52	101.10	100.02	100.52	100.11	101.88	101.45	100.52	100.64	100.25
Structural formulae based on 24 oxygens											
Si	5.921	5.852	5.890	5.865	5.898	5.899	5.908	5.887	5.889	5.920	5.922
Al^{IV}	0.079	0.148	0.110	0.135	0.102	0.101	0.092	0.113	0.111	0.080	0.078
Al^{VI}	1.298	1.686	1.599	1.425	1.346	1.698	1.267	2.775	3.178	3.465	3.194
Ti	0.196	0.187	0.076	0.130	0.106	0.157	0.142	0.132	0.053	0.013	0.030
Fe^{3+}	2.389	2.090	2.320	2.451	2.536	2.090	2.493	1.076	0.741	0.591	0.759
Fe^{2+}	0.186	0.083	-	0.121	-	0.074	0.076	0.071	-	0.020	-
Mn	0.073	0.060	-	-	0.069	-	0.022	-	-	0.019	-
Mg	0.029	-	-	-	-	-	0.026	-	0.023	-	-
Ca	5.829	5.895	6.025	5.875	5.948	5.981	5.998	5.947	6.049	5.892	6.049
R^{3+}	3.883	3.963	3.995	4.006	3.988	3.945	3.902	3.983	3.972	4.069	3.983
R^{2+}	6.117	6.037	6.025	5.996	6.017	6.055	6.122	6.018	6.072	5.931	6.049
Mole percent end-members											
And†	63.39	56.56	59.64	64.55	65.87	55.68	64.56	30.10	19.62	15.25	19.57
Gross	31.90	41.08	40.36	33.43	32.99	43.10	33.41	68.73	80.00	84.08	80.43
Alm	3.03	1.38	-	2.02	-	1.22	1.25	1.17	-	0.34	-
Spess	1.20	0.99	-	-	1.14	-	0.35	-	-	0.33	-
Pyr	0.48	-	-	-	-	-	0.43	-	0.38	-	-
$Al^{VI}/Al^{VI}+Fe^{3+}$	0.352	0.447	0.408	0.368	0.347	0.448	0.337	0.721	0.811	0.854	0.808

* Distance from the igneous contact

** Fe_2O_3 based on 16 cations

T11A and T12 are from the South Kootingal locality. All other samples are from Horse Arm Creek.

† And = andradite, Gross = grossular, alm = almandine, spess = spessartine, pyr = pyrope.

TABLE 4.4. Microprobe analyses of clinopyroxenes (with garnet) in impure calcareous rocks

	Calcareous Litharenites					Impure Calcirudites			
Sample No.	T103-2	T132A-1	T83B	T80	T81B	371B	371-1	T11A	T12
Distance (m)*	950	750	450	100	75	350	350	600	700
SiO_2	51.94	49.85	51.45	50.40	50.00	50.82	52.70	51.63	52.30
TiO_2	-	-	-	0.17	-	-	-	-	-
Al_2O_3	0.34	0.30	0.52	2.61	0.67	1.06	0.60	0.93	0.72
Fe_2O_3**	0.53	0.27	1.14	3.30	1.46	1.38	1.38	1.23	0.18
FeO	11.50	20.76	14.98	11.11	16.08	15.52	5.85	12.53	10.76
MnO	0.73	-	-	-	0.51	-	-	0.21	-
MgO	10.28	4.76	8.31	8.85	6.74	7.72	13.44	9.36	11.04
CaO	24.70	23.72	24.25	22.87	23.99	24.30	25.61	24.27	25.07
Na_2O	-	-	0.15	0.92	0.16	-	0.17	0.27	-
Total	100.02	99.65	100.80	100.23	99.62	100.80	99.75	100.43	100.07
Structural formulae based on 6 oxygens									
Si	1.984	1.989	1.977	1.923	1.966	1.959	1.970	1.971	1.981
Al^{IV}	0.015	0.011	0.023	0.077	0.031	0.041	0.026	0.029	0.019
Al^{VI}	-	0.003	-	0.040	-	0.007	-	0.013	0.013
Ti	-	-	-	0.005	-	-	-	-	-
Fe^{3+}	0.015	0.008	0.033	0.095	0.043	0.040	0.039	0.035	0.005
Fe^{2+}	0.367	0.693	0.482	0.355	0.529	0.500	0.183	0.400	0.341
Mn	0.024	-	-	-	0.017	-	-	0.007	-
Mg	0.585	0.283	0.476	0.503	0.395	0.444	0.749	0.533	0.623
Ca	1.011	1.014	0.998	0.935	1.011	1.004	1.026	0.993	1.018
Na	-	-	0.011	0.068	0.012	-	0.123	0.020	-
$Mg/Mg+Fe^{2+}$	0.614	0.290	0.497	0.587	0.428	0.470	0.805	0.571	0.647

* Distance from the igneous contact.

** Fe_2O_3 calculated by method of Papike *et al.* (1974).

T11A and T12 are from the South Kootingal locality. All other samples are from the Horse Arm Creek locality.

4.5.5 Epidote

Epidote compositions remain very similar regardless of their mineral association (Table 4.5). $Al/Al+Fe^{3+}$ ratios in the epidotes are typically between 0.70 and 0.75.

4.5.6 Plagioclase

Outside the aureole and within the biotite zone, plagioclase occurs only as crystal fragments that are relicts of the original sediment. These fragments vary in composition from An 40 to An 60. Metamorphic plagioclase, with a granoblastic-polygonal texture is first evident at the clinopyroxene isograd, and this plagioclase is typically around An 25. Although present in the clinopyroxene zone, metamorphic plagioclase is not abundant until the garnet zone. Both metamorphic and relict plagioclase occur throughout the garnet and wollastonite zones, and the metamorphic plagioclase is consistently more-albitic (An 20-30) than the associated relict crystals, which continue to have values of An 40 to An 60.

Within the wollastonite + plagioclase zone, most plagioclase forms part of the granoblastic-polygonal assemblage and is oligoclase-andesine in composition (commonly An 30 - An 35), though minor relict grains (An 40 - An 50) still exist. Metamorphic plagioclase with An values significantly higher than An 30-35 can occur in apparent equilibrium with wollastonite in the higher-grade parts of the wollastonite + plagioclase zone. A value as high as An 80 was recorded at a distance of 50 metres from the contact (sample T116).

4.6 METAMORPHIC REACTIONS AND PHASE RELATIONS

4.6.1 Introduction

The most complete study of the mineralogy and mineral chemistry in the various metamorphic zones has been established in the calcareous litharenites. The following reactions are based primarily on this type of rock. However, they are also considered to be broadly appropriate to the metamorphic changes occurring in the matrix material of the impure calcirudites.

The mineralogy of the metamorphic zones is represented on a series of

TABLE 4.5. Microprobe analyses of epidotes in impure calcareous rocks

Associated Minerals*	Chl Bi	Chl Ci	Chl Amph	Cpx	Gt
Sample No.	T31-1	T31-2	T95A-2	T26-1	T103
SiO_2	37.97	37.97	37.90	37.39	37.46
TiO_2	-	-	-	0.29	0.34
Al_2O_3	23.63	22.96	24.40	23.59	23.11
Fe_2O_3†	12.52	14.02	12.56	13.20	14.88
FeO	0.97	0.02	-	-	-
MnO	-	-	0.28	-	-
MgO	0.11	0.23	0.17	0.11	0.11
CaO	22.77	23.34	23.39	23.68	23.86
Total	97.97	98.54	98.70	98.26	99.76
Structural formulae based on 25 oxygens					
Si	6.038	6.018	5.972	5.940	5.897
Al^{IV}	-	-	0.028	0.060	0.103
Al^{VI}	4.429	4.289	4.503	4.358	4.185
Ti	-	-	-	0.035	0.040
Fe^{3+}	1.498	1.673	1.489	1.578	1.763
Fe^{2+}	0.129	0.003	-	-	-
Mn	-	-	0.037	-	-
Mg	0.026	0.054	0.040	0.026	0.026
Ca	3.879	3.964	3.949	4.031	4.024
$Al^{VI}/Al^{VI}=Fe^{3+}$	0.747	0.719	0.751	0.734	0.704

† Fe_2O_3 calculated on the basis of 16 cations

* Chl = chlorite, bi = biotite, amph = amphibole, cpx = clinopyroxene, gt = garnet

T95A, T103 are calcareous litharenites from the Horse Arm Creek locality. T26, T31 are impure calcirudites from the South Kootingal locality.

ACF diagrams in Fig. 4-5, A→G. General equations (unbalanced) representing the mineralogical changes between the zones are also shown. In the garnet-bearing zones $CaO-Al_2O_3-SiO_2$ diagrams are also shown to more clearly depict the reactions taking place. A $CaO-NaAlSi_3O_8-CaAl_2Si_2O_8$ diagram is shown for the wollastonite + plagioclase zone, to depict the dependence of the mineral assemblage on the An content of the plagioclase.

Reactions within the impure biomicrites are briefly considered in Section 4.6.3. Insufficient data are available on the stylolitic limestones to establish metamorphic reactions. However a discussion is given in Section 4.6.4 on the distinct mineralogy of the stylolitic limestones, in relation to a comparison between the bulk-rock composition of the stylolitic limestones and that of the other impure calcareous rocks studied.

4.6.3 Calcareous Litharenites

Outside the Aureole

The general mineralogy in the calcareous litharenites outside the aureole has been discussed in Section 4.4.2, and is represented in Fig. 4-5A.

Biotite Isograd

Textural evidence (Section 4.4.2 and Plates 4-1B and C) suggests that biotite has formed from previous chlorite, commonly in close association with either epidote or amphibole. In this zone, chlorite + calcite is stable relative to epidote + amphibole (Fig. 4-5B). The biotite has a lower Mg/Mg+Fe ratio than its precursor chlorite (Section 4.5.2). However, the immediate loss of K-feldspar, and the lack of a consistent change in the chlorite composition across the biotite isograd, suggest that this is a discontinuous reaction. From probe data on the phases a possible balanced equation to represent the formation of biotite plus amphibole is

1.00 Chlorite + 3.16 K-feldspar + 0.71 Calcite + 0.26 Hematite + 0.20 Sphene → 1.50 Biotite + 0.46 Amphibole + 1.56 Al_2O_3 + 3.61 Quartz + 0.71 CO_2 + 4.54 H_2O (4-I)

Figure 4-5: ACF diagrams for the calcareous lithareneites at the Horse Arm Creek locality.

Symbols $A = Al_2O_3 + Fe_2O_3$

$C = CaO$

$F = FeO + MnO + MgO$

All oxides expressed in molecular proportions.
Mineral compositions are based on probe analyses.
All assemblages below the garnet isograd contain Fe oxides, whereas those above are virtually opaque free (see text).
General equations for the mineralogical changes between the zones are shown. Balanced equations for these changes are given in the text.

In the garnet-bearing zones $CaO - Al_2O_3 - SiO_2$ diagrams are shown.
The Al_2O_3 components includes both Al_2O_3 and Fe_2O_3.
These diagrams more clearly depict the reactions taking place at higher grade.

A $CaO - NaAlSi_3O_8 - CaAl_2Si_2O_8$ diagram is shown for the wollastonite + plagioclase zone. Garnet is plotted in this diagram by combining Al_2O_3 and Fe_2O_3 as a single component.

Amph = amphibole; Bi - biotite; Cal = calcite;
Chl = chlorite; Cpx = clinopyroxene; Ep = epidote;
Gt = garnet; K-f = K-feldspar; Plag = plagioclase;
Qtz = quartz; Woll = wollastonite.

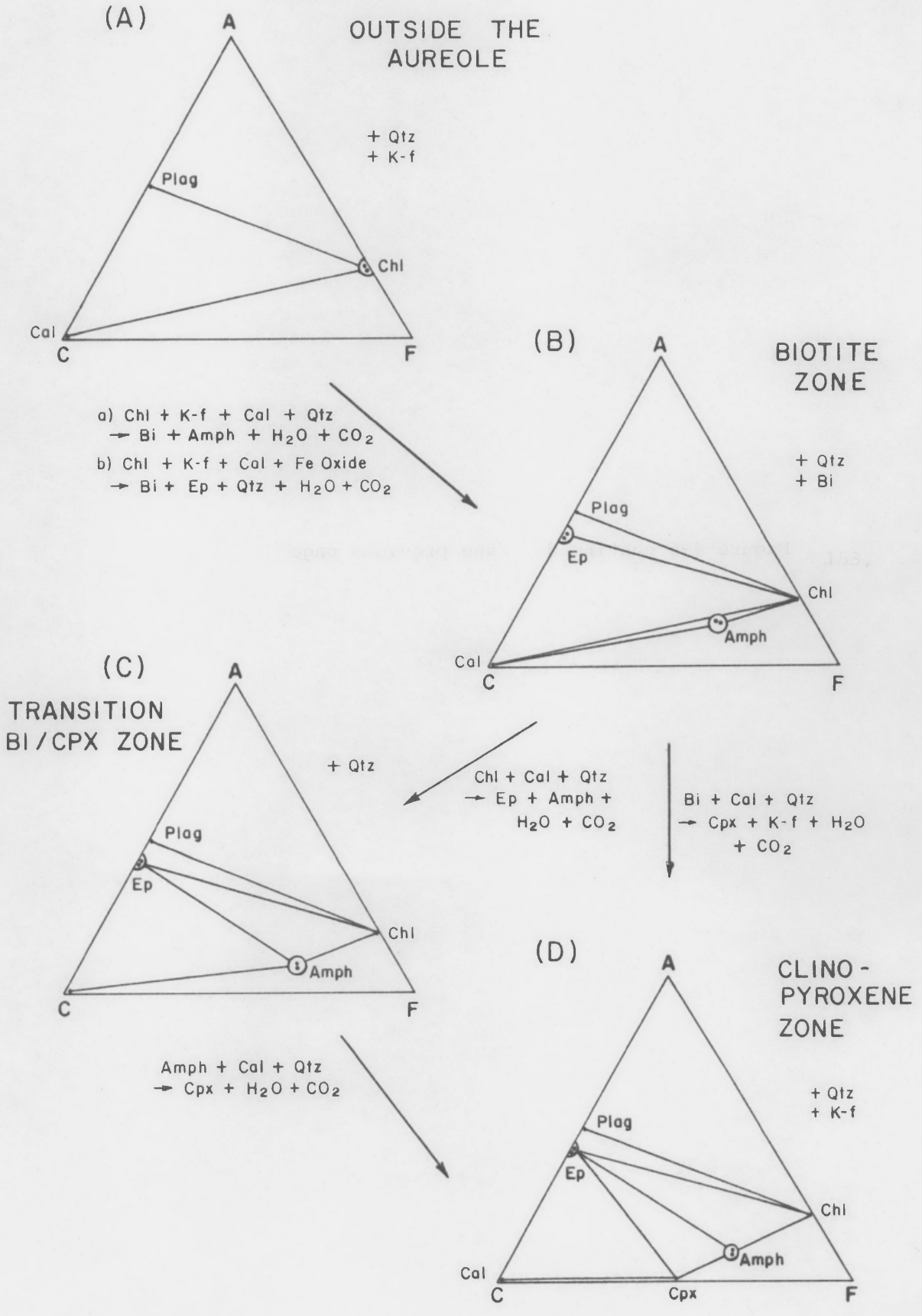
(A)
A
OUTSIDE THE AUREOLE
+ Qtz
+ K-f
Plag
Chl
Cal
C
F
a) Chl + K-f + Cal + Qtz → Bi + Amph + H_2O + CO_2
b) Chl + K-f + Cal + Fe Oxide → Bi + Ep + Qtz + H_2O + CO_2
(B)
A
BIOTITE ZONE
+ Qtz
+ Bi
Plag
Ep
Chl
Amph
Cal
C
F
(C)
A
TRANSITION BI/CPX ZONE
+ Qtz
Plag
Ep
Chl
Amph
C
F
Chl + Cal + Qtz → Ep + Amph + H_2O + CO_2
Bi + Cal + Qtz → Cpx + K-f + H_2O + CO_2
Amph + Cal + Qtz → Cpx + H_2O + CO_2
(D)
A
CLINO-PYROXENE ZONE
+ Qtz
+ K-f
Plag
Ep
Chl
Amph
Cal
C
Cpx
F

Figure 4-5 continued: see previous page

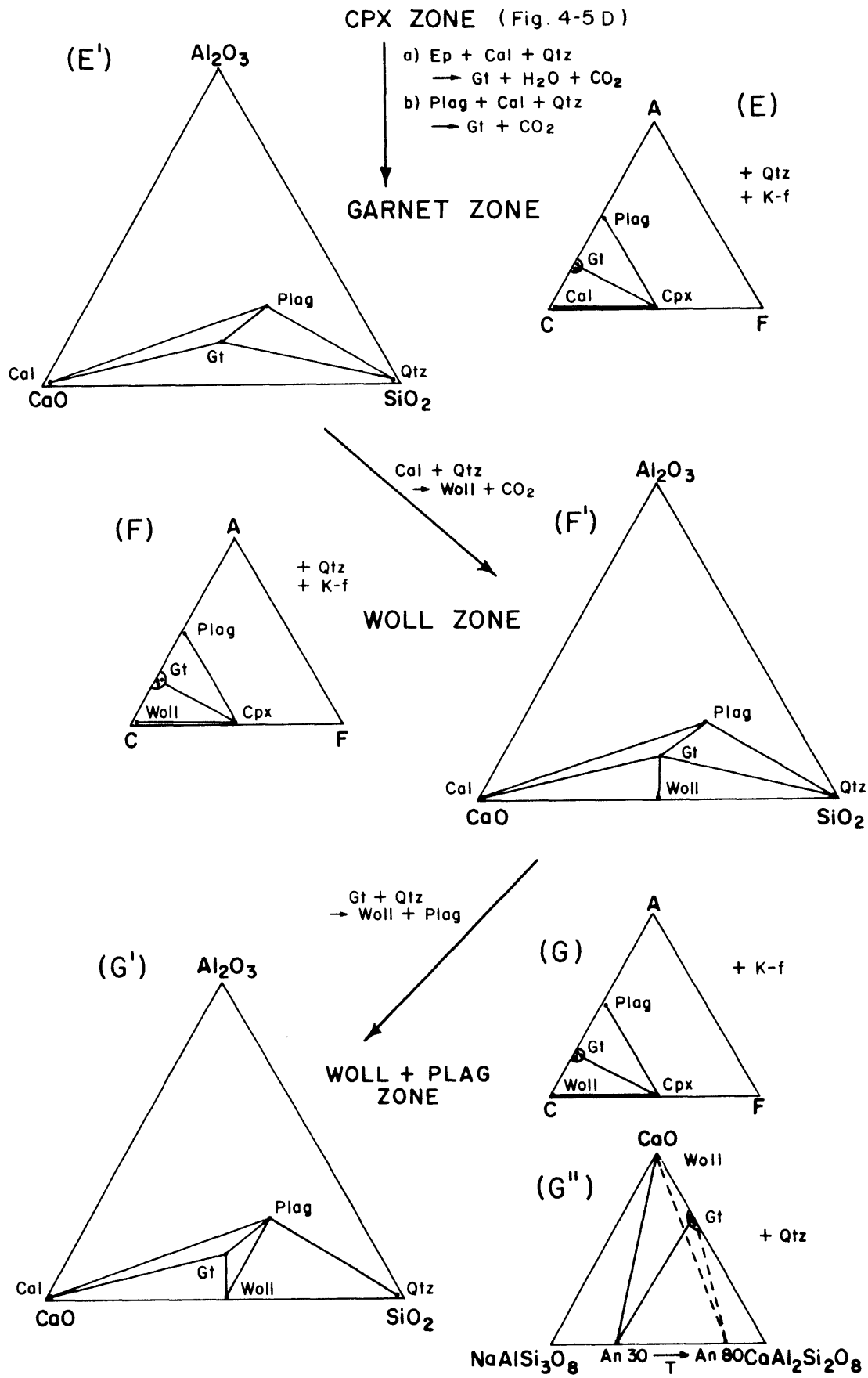
CPX ZONE (Fig. 4-5 D)
(E')
Al_2O_3
a) Ep + Cal + Qtz → Gt + H_2O + CO_2
b) Plag + Cal + Qtz → Gt + CO_2
GARNET ZONE
(E)
A
+ Qtz
+ K-f
Plag
Gt
Cal
Cpx
C
F
Plag
Gt
Cal
Qtz
CaO
SiO_2
Cal + Qtz → Woll + CO_2
(F)
A
+ Qtz
+ K-f
Plag
Gt
Woll
Cpx
C
F
WOLL ZONE
(F')
Al_2O_3
Plag
Gt
Woll
Cal
Qtz
CaO
SiO_2
Gt + Qtz → Woll + Plag
(G')
Al_2O_3
Plag
Gt
Woll
Cal
Qtz
CaO
SiO_2
WOLL + PLAG ZONE
(G)
A
+ K-f
Plag
Gt
Woll
Cpx
C
F
(G'')
CaO
Woll
Gt
+ Qtz
$NaAlSi_3O_8$
An 30 → An 80
T
$CaAl_2Si_2O_8$

REACTANTS

Chlorite $Al_{2.55}Fe_{3.89}Mn_{.04}Mg_{5.55}Si_{5.30}Al_{2.70}O_{20}(OH)_{16}$

K-feldspar $K_{.95}Na_{.05}AlSi_3O_8$

Sphene $CaTiSiO_5$

PRODUCTS

Biotite $K_{2.00}Al_{.50}Ti_{.13}Fe_{2.31}Mg_{2.93}Si_{5.50}Al_{2.50}O_{20}(OH)_4$

Amphibole $Na_{.25}Ca_{1.90}Al_{.42}Fe^{3+}_{.58}Fe^{2+}_{1.48}Mn_{.02}Mg_{2.51}Si_{6.78}Al_{1.22}O_{22}(OH)_2$

The excess Al_2O_3 in the products may react with quartz, plus further Fe oxide and calcite to give epidote:

$$1.56\ Al_2O_3 + 0.62\ \text{Hematite} + 2.89\ \text{Calcite} + 4.38\ \text{Quartz} + 0.73\ H_2O \rightarrow 0.73\ \text{Epidote} + 2.89\ CO_2 \qquad (4\text{-IA})$$

Epidote $Ca_{3.96}Al_{4.28}Fe_{1.67}Si_6O_{24}(OH)_2$.

However, epidote is not found in association with amphibole, as noted in Section 4.4.2. A possible balanced equation for the formation of biotite plus epidote is

$$1.00\ \text{Chlorite} + 3.55\ \text{K-feldspar} + 0.66\ \text{Hematite} + 1.80\ CaCO_3 + 0.26\ \text{Sphene} \rightarrow 1.97\ \text{Biotite} + 0.52\ \text{Epidote} + 2.46\ SiO_2 + 1.80\ CO_2 + 3.54\ H_2O \qquad (4\text{-II})$$

REACTANTS

Chlorite $Al_{2.30}Fe_{2.70}Mg_{6.90}Si_{5.70}Al_{2.30}O_{20}(OH)_{16}$

K-feldspar $KAlSi_3O_8$

Sphene $CaTiSiO_5$

PRODUCTS

Biotite $K_{1.80}Al_{.60}Ti_{.13}Fe_{1.70}Mg_{3.50}Si_{5.60}Al_{2.40}O_{20}(OH)_4$

Epidote $Ca_{3.96}Al_{4.28}Fe_{1.67}Si_{6.00}O_{24}(OH)_2$

In equation 4-I, the lower Mg/Mg+Fe ratio of the biotite compared to chlorite is balanced primarily by the formation of amphibole, whereas in equation 4-II, Fe oxide is believed to be an important reacting phase.

Clinopyroxene Isograd

The incoming of clinopyroxene is associated with the reappearance of K-feldspar, now having a granoblastic texture, and the immediate loss

of biotite. An equation representing this reaction is given by Thompson (1975b, p. 120) as

(FeMg) Biotite + 3 Calcite + 6 Quartz = 3(MgFe) Clinopyroxene + K-feldspar + H_2O + $3CO_2$

In Fig. 4-5 this is shown as the equation relating the biotite and clinopyroxene zones (Figs. 4-5B and D). Thompson (1975b) considered this to be a continuous reaction, and represented it on a T-X(Mg-Fe) diagram as a divariant loop (Thompson, 1975b, Fig. 8), with the loop designating the relative Mg/Mg+Fe ratios of the coexisting biotite and clinopyroxene. This diagram is schematically reproduced here as Fig. 4-6. With increasing temperature, both the biotite and clinopyroxene would be expected to shift to lower Mg/Mg+Fe ratios. However, in the impure calcareous rocks of this study, biotite and clinopyroxene do not appear to coexist. Therefore, as with reactions 4-I and 4-II, this reaction is believed to be discontinuous, with the higher Mg content of the clinopyroxene compared to the biotite being balanced by the associated formation of minor epidote and Fe oxide. Therefore a balanced equation based on probe data is suggested as

1.00 Biotite + 5.56 Calcite + 11.03 Quartz
→ 4.51 Clinopyroxene + 2.00 K-feldspar + 0.23 Epidote + 0.13 Sphene
+ 0.18 Hematite + 1.77 H_2O + 5.56 CO_2 (4-III)

REACTANTS

Biotite $K_{2.00}Al_{.50}Ti_{.13}Fe_{2.31}Mg_{2.93}Si_{5.50}Al_{2.50}O_{20}(OH)_4$

PRODUCTS

Clinopyroxene $Ca_{1.00}Fe^{3+}_{.05}Fe^{2+}_{.30}Mg_{.65}Si_2O_6$

K-feldspar $KAlSi_3O_8$

Epidote $Ca_{4.00}Al_{4.36}Fe_{1.58}Si_6O_{24}(OH)_2$

Sphene $CaTiSiO_5$

Fig. 4-6 shows that the biotite → clinopyroxene + K-feldspar reaction is not applicable to the full range of biotite Mg/Mg+Fe values, at least at the conditions designated; Mg-rich biotite breaks down to form tremolite + K-feldspar at lower temperatures (reaction 7 of Thompson, 1975b, p.120). This reaction has been described by several authors concerned with pure-Mg phases in calcareous systems (e.g. Hoschek, 1973;

Figure 4-6: Schematic T-X(Fe-Mg) diagram for the reaction

$Bi + Cal + Qtz \rightarrow Cpx + K\text{-}f + H_2O + CO_2$

This figure is reproduced in part from Thompson (1975b, Fig.8).

Act = actinolite, Ann = annite, Cal = calcite, Cpx = clinopyroxene, Diop = diopside, Hed = hedenbergite, K-f = K-feldspar, Phl = phlogopite, Trem = tremolite, Qtz = quartz.

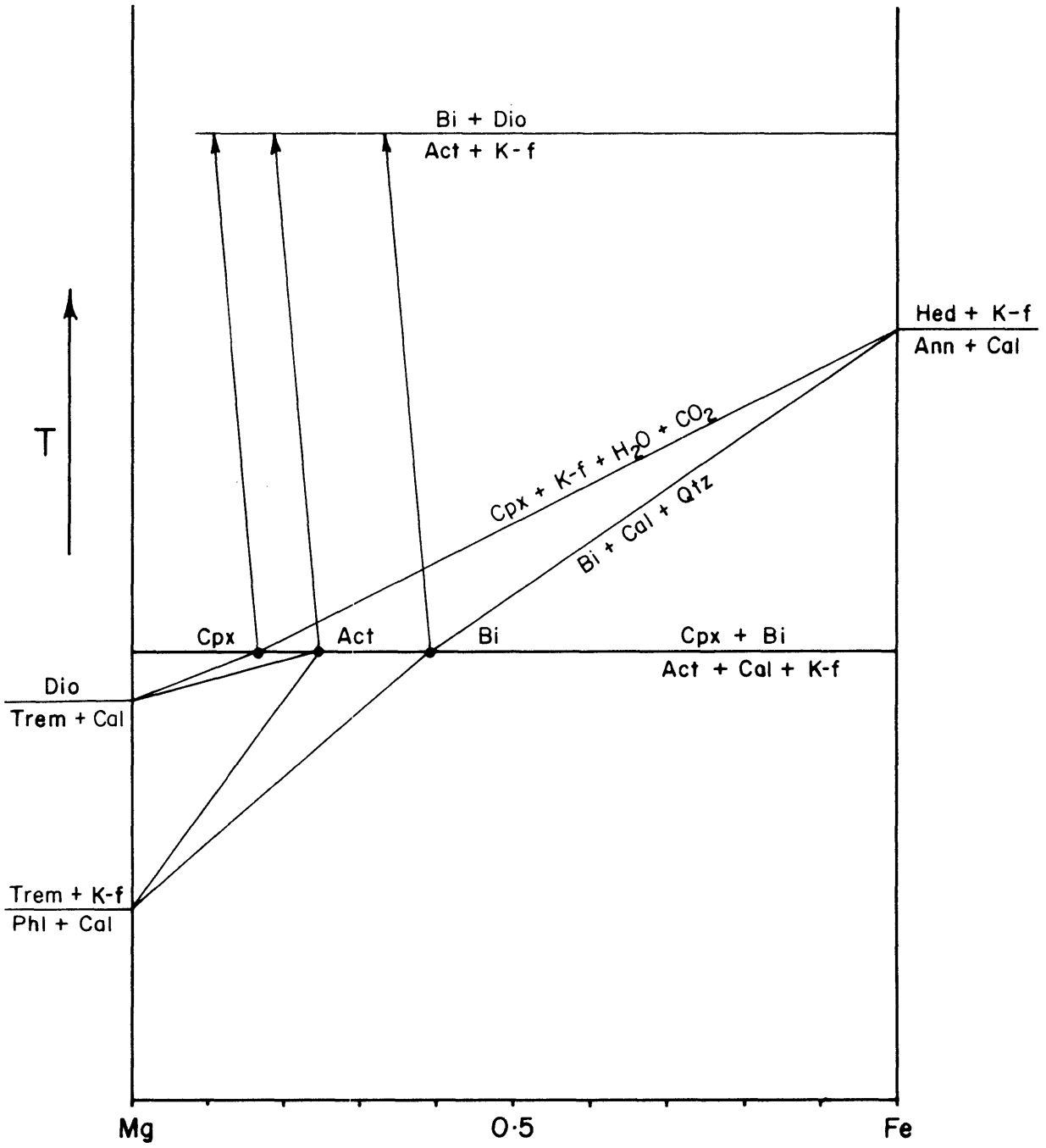
Bi + Dio
Act + K-f
Hed + K-f
Ann + Cal
T
Cpx + K-f + H2O + CO2
Bi + Cal + Qtz
Cpx
Act
Bi
Cpx + Bi
Act + Cal + K-f
Dio
Trem + Cal
Trem + K-f
Phl + Cal
Mg
0·5
Fe

Rice, 1977). However, no evidence of it exists in the rocks studied here, assumedly because the Fe content of the biotite is too high under the relevant metamorphic conditions (discussed further in Section 4.7.2).

In the clinopyroxene zone, evidence remains of the formation of epidote + amphibole from chlorite + calcite (Section 4.4.2). This results in a change in the topology of the ACF triangles (Figs. 4-5B and C). A general equation for this reaction has been given by Deer *et al.* (1972, P.67):

3(Fe,Mg) Chlorite + 10 Calcite + 21 Quartz → 2 Clinozoisite + 3(Fe,Mg) Amphibole + 10 CO_2 + 8 H_2O.

From probe data on coexisting epidote, amphibole and chlorite in the clinopyroxene zone, two possibilities arise for a balanced equation representing this reaction. If the chlorite is relict and its composition has been unaffected by the reaction, then a discontinuous reaction represented by equation 4-IVA is appropriate:

1.00 Chlorite + 9.71 Calcite + 9.09 Quartz + 5.83 Plagioclase
→ 3.41 Epidote + 0.88 Amphibole + 9.71 CO_2 + 3.71 H_2O (4-IVA)

REACTANTS

Chlorite $Al_{2.59}Fe_{6.41}Mn_{.03}Mg_{2.91}Si_{5.4}Al_{2.6}O_{20}(OH)_{16}$

Plagioclase $Ca_{.94}Na_{.06}Al_{1.94}Si_{2.06}O_8$

PRODUCTS

Epidote $Ca_{3.95}Al_{4.50}Fe_{1.49}Mn_{.01}Si_6O_{24}(OH)_2$

Amphibole $Na_{.38}Ca_{1.96}Al_{.18}Fe^{3+}_{.52}Fe^{2+}_{.99}Mn_{.02}Mg_{3.30}Si_{6.86}Al_{1.14}O_{22}(OH)_2$

However, the chlorite is more Fe-rich than those typically present at lower grade. Therefore, a continuous reaction involving the shift of the chlorite Mg/Mg+Fe ratio to lower values may have occurred:

1.0 Chlorite(1) + 6.09 Calcite + 7.17 Quartz + 1.82 Plagioclase
→ 0.2 Chlorite(2) + 1.38 Epidote + 1.05 Amphibole + 6.09 CO_2 + 3.97 H_2O (4-IVB)

REACTANTS

Chlorite(1) $Al_{2.77}Fe_{4.93}Mn_{.03}Mg_{4.05}Si_{5.35}Al_{1.65}O_{20}(OH)_{16}$

Plagioclase $Ca_{.78}Na_{.22}Al_{1.78}Si_{2.22}O_8$

PRODUCTS

Chlorite(2) $Al_{2.59}Fe_{6.41}Mn_{.03}Mg_{2.91}Si_{5.4}Al_{2.6}O_{20}(OH)_{16}$

Epidote $Ca_{3.59}Al_{4.50}Fe_{1.59}Mn_{.01}Si_{6}O_{24}(OH)_{2}$

Amphibole $Na_{.38}Ca_{1.96}Al_{.18}Fe^{2+}_{.52}Fe^{3+}_{.99}Mn_{.02}Mg_{3.30}Si_{6.86}Al_{1.14}O_{22}(OH)_{2}$

The lower Fe content of the chlorite, though, may represent only a variation in host-rock chemistry. Further probe data would be required to verify which of the above reactions is more likely. The assemblage epidote + amphibole was not recognised outside the clinopyroxene zone; nevertheless, the breakdown of chlorite + calcite to epidote + amphibole has been experimentally shown to occur at lower temperatures than those required for the incoming of clinopyroxene (see discussion of Figs. 4-7, 4-8 and 4-9 in Section 4.7.2). Hence, Fig. 4-5C represents a possible transition zone between the biotite and clinopyroxene zones.

Textural evidence also exists in the clinopyroxene zone for the instability of calcite + amphibole (Section 4.4.2). The reaction for the breakdown of calcite + amphibole presented by Thompson (1975b, p.120, reaction 3) is

(Fe,Mg) Amphibole + 3 Calcite + 2 Quartz → 5 (Mg,Fe) clinopyroxene + 3 CO_2 + H_2O.

Amphibole compositions within the clinopyroxene zone are not distinctly different from those in the biotite zone. Therefore, a balanced equation based on probe data is suggested as

1.0 Amphibole + 3.40 Calcite + 4.17 Quartz
→ 4.44 Clinopyroxene + 3.40 CO_2 + 0.76 H_2O + 0.24 Epidote + 0.25 Albite (4-V)

REACTANTS

Amphibole $Na_{.25}Ca_{2.00}Al_{.20}Fe^{3+}_{.47}Fe^{2+}_{1.55}Mg_{2.75}Si_{6.9}Al_{1.10}O_{22}(OH)_{2}$

PRODUCTS

Clinopyroxene $Ca_{1.00}Fe^{3+}_{.05}Fe^{2+}_{.32}Mg_{.63}Si_{2}O_{6}$

Epidote $Ca_{4.00}Al_{4.36}Fe_{1.58}Si_{6}O_{24}(OH)_{2}$

However, if the amphibole involved in this reaction coexisted with epidote at lower grade (i.e. formed via either reactions 4-IVA or 4-IVB), it would be expected to have higher Mg/Mg+Fe ratios than those recorded in the biotite zone (Section 4.5.2). The subsequent breakdown of amphibole +

calcite to clinopyroxene may then have taken place as a continuous reaction, forming a more Fe-rich amphibole in the products rather than the epidote shown in equation 4-V.

A combination of the reactions proposed above yields the various mineral assemblages characteristic of the clinopyroxene zone (Fig. 4-5D). These various assemblages often occur within a single thin section, owing to the small-scale compositional variations inherent within these rocks. Reactions 4-IVA and B and 4-V would involve increases in the Na content of the plagioclase, consistent with the incoming of metamorphic plagioclase (An 20-30), derived from the breakdown of relict plagioclase (An 40-60), across the clinopyroxene isograd (Section 4.5.6).

Garnet Isograd

The garnet zone is characterised by the formation of garnet + clinopyroxene assemblages. Major decreases in the modal contents of epidote and opaque oxides occur across the garnet isograd; rocks in the garnet zone are virtually free of opaques. Detrital crystal fragments of calcite are also absent, and the assemblage plagioclase + calcite + quartz is apparently unstable. These features have been discussed in Section 4.4.2. General reactions, based on Al end members, appropriate to these petrographic changes are

1) 2 Zoisite + 5 Calcite + 3 Quartz → 3 Grossular + 5 CO_2 + H_2O and

2) Anorthite + 2 Calcite + 3 Quartz → Grossular + 2 CO_2.

These reactions have been established by Kerrick *et al.* (1973) and Kerrick (1974) for the CaO-Al_2O_3-SiO_2-CO_2-H_2O system. Using probe data on the garnet and epidote, to allow for Fe_2O_3 substitution, balanced equations for these reactions are given as 4-VI and 4-VII respectively:

1.00 Epidote + 10.94 Calcite + 8.67 Quartz + 2.01 Hematite

→ 2.49 Garnet + 10.94 CO_2 + 1.00 H_2O (4-VI)

REACTANTS

Epidote $Ca_{4.00}Al_{4.25}Fe^{3+}_{1.76}Si_{6.00}O_{24}(OH)_2$

PRODUCTS

Garnet $Ca_{6.00}Al_{1.60}Fe^{3+}_{2.32}Si_{5.89}Al_{.11}O_{24}$

and 1.00 Anorthite + 6.02 Calcite + 4.89 Quartz + 1.35 Hematite

→ 1.17 Garnet + 6.02 CO_2 (4-VII)

PRODUCTS

Garnet $Ca_{6.00}Al_{1.60}Fe^{3+}_{2.32}Si_{5.89}Al_{.11}O_{24}$.

A combination of these reactions yields the assemblages portrayed in the ACF and $CaO-Al_2O_3-SiO_2$ diagrams of Figs. 4-5E and 4-5E' respectively.

The anorthite required in reaction 4-VII is believed to have been derived from the continued breakdown of relict plagioclase (An 40-60) to metamorphic plagioclase (An 20-30). This is consistent with a marked increase in metamorphic plagioclase across the garnet isograd (Section 4.5.6).

The breakdown of epidote to garnet (via raction 4-VI) is believed to be a discontinuous reaction, with the lower Mg/Mg+Fe ratio of the garnet compared to epidote being balanced by the obvious decrease in Fe oxide at the garnet isograd. Although epidote (? retrograde) and garnet coexist in the outer part of the garnet zone (Section 4.4A), no evidence of a systematic change in garnet composition occurs within this zone (Section 4.5.3). Similarly, the petrographical changes described above occur abruptly at the garnet isograd, rather than across the field of epidote and garnet coexistence. Therefore, the coexistence of epidote and garnet is not believed to indicate a continuous reaction.

A common feature in the garnet zone is the presence of sphene rims on rutile. This suggests a reaction between rutile, calcite and quartz has taken place to form sphene. The rutile has possibly resulted from the breakdown of opaque oxides, with their Fe oxide component being used in the formation of garnet (e.g. reactions 4-VI,VII and VIII).

Wollastonite Isograd

Without extensive change in the texture of the rocks, original grains of quartz and remaining patches of calcite are converted to wollastonite. The boundary is represented by the reaction

Calcite + Quartz → Wollastonite + CO_2 (4-VIII)

No evidence was found of the three-phase assemblage calcite + quartz + wollastonite.

Calcite, which remained after garnet formation, is totally consumed at this boundary, while quartz remains as part of the fine-grained felsic matrix.

Wollastonite + Plagioclase Isograd

This boundary is designated by the stability of wollastonite + plagioclase, and the formation of an almost entirely metamorphic texture (Section 4.4.2). A commonly proposed general reaction for the incoming of wollastonite + plagioclase (anorthite) is

Grossular + Quartz → 2 Wollastonite + Anorthite

(Newton, 1966). This is shown in the $CaO-Al_2O_3-SiO_2$ diagram (Fig. 4-5G'). Garnet compositions in this zone are similar to those in the garnet and wollastonite zones, with compositions around Gr 40, while plagioclase compositions typically range from An 30 to An 35. Quartz appears to be absent from the wollastonite + plagioclase zone in these rocks. Therefore, this isograd can be represented by the equation

Garnet (Gr 40) + Quartz → 2 Wollastonite + Plagioclase (An 30) (4-IX).

The anorthite content of metamorphic plagioclase has slightly increased across the wollastonite + plagioclase isograd (An 20-30 → An 30-35), and a possible balanced equation for reaction 4-IX is

1.0 Garnet + 0.97 Quartz + 6 Plagioclase(1)
→ 5.14 Wollastonite + 6.46 Plagioclase(2) + 1.16 Fe_2O_3 (4-IXA)

REACTANTS

Garnet $Ca_{6.0}Al_{1.6}Fe_{2.32}Si_{5.89}Al_{.11}O_{24}$

Plagioclase(1) $Na_{.8}Ca_{.2}Al_{1.2}Si_{2.8}O_8$

PRODUCTS

Wollastonite $CaSiO_3$

Plagioclase(2) $Na_{.7}Ca_{.3}Al_{1.3}Si_{2.7}O_8$

However, several major inconsistencies exist between this reaction and the mineralogical changes observed. No opaque oxides occur within the wollastonite + plagioclase zone, and no increase is evident in the Fe contents of either garnet or clinopyroxene (though such variations in mineral chemistry could be masked by variations in host-rock chemistry), to accommodate the excess iron oxide derived in equation 4-XA. Similarly, no obvious modal decrease in garnet occurs across this boundary, nor is there a significant increase in wollastonite. In addition much relict plagioclase (An 50-60) has recrystallised to metamorphic plagioclase (An 30-35) (Section 4.4.2), involving a decrease in anorthite content, in

contrast to the increase expected with the breakdown of garnet.

Although reaction 4-IXA may have taken place to a small degree, the most obvious mineralogical changes across the wollastonite + plagioclase isograd can be represented simply by the re-equilibration of plagioclase:

6 Metamorphic Plagioclase(1) + 3 Relict Plagioclase → 9 Metamorphic Plagioclase(2) (4-IXB)

REACTANTS

Metamorphic Plagioclase(1) $Na_{.8}Ca_{.2}Al_{1.2}Si_{2.8}O_8$

Relict Plagioclase $Na_{.5}Ca_{.5}Al_{1.5}Si_{2.5}O_8$

PRODUCTS

Metamorphic Plagioclase(2) $Na_{.7}Ca_{.3}Al_{1.3}Si_{2.7}O_8$

This reaction requires no change in the modal contents of garnet or wollastonite and no change in the composition of garnet. Thus the plagioclase in the wollastonite + plagioclase zone has re-equilibrated with the co-existing wollastonite, whereas in the wollastonite zone there is no textural evidence of equilibration between wollastonite and plagioclase. Although the actual mineralogical changes across this isograd are not accurately represented by equation 4-IX, this equation is still relevant, because temperatures above that required for reaction 4-IX to proceed to the right must have been attained in the wollastonite + plagioclase zone. This conclusion is used to estimate appropriate temperatures for this zone in Section 4.7.2. Plagioclase with An values significantly higher than An 30 have been recorded in apparent equilibrium with wollastonite at higher grades in the wollastonite + plagioclase zone. Plagioclase compositions range from An 30 to An 80, the latter being recorded close to the contact of the Inlet Monzonite (Section 4.5.6), which is represented on the $CaO\text{-}NaAlSi_3O_8\text{-}CaAl_2Si_2O_8$ diagram (Fig. 4-5G"). Therefore, the stability of wollastonite + plagioclase appears to be divariant with regard to the An content of the plagioclase.

4.6.3 Impure Biomicrites

The two major mineralogical changes within the impure biomicrites (Section 4.4.4) can be represented in a general form by the reactions

1) Biotite + Calcite → Clinopyroxene + K-feldspar + H_2O + CO_2,

and at higher grade

2) Calcite + Quartz → Wollastonite + CO_2.

Examples of these reactions have been discussed above.

4.6.4 Discussion of the Mineralogy and Bulk-Rock Composition of the Stylolitic Limestones

In this chapter, metamorphic zones (Section 4.4.1) and reactions marking the zone boundaries (outlined above) have been defined on the appearance and disappearance of mineral assemblages appropriate to the system $K_2O(Na_2O)$-CaO-MgO(FeO)-$Al_2O_3(Fe_2O_3)$-SiO_2-H_2O-CO_2. However, the mineralogy of the non-carbonate part of the stylolitic limestones (Section 4.4.5) is distinct, and appears to correlate with a bulk-rock composition that is lower in SiO_2 and Al_2O_3 than the other rock types studied, and contains only minor, if any, K_2O.

The stylolitic limestones consist mainly of calcite with stringers of non-carbonate material. In the outer part of the aureole north of the Inlet Monzonite, sample T104 contains stringers of minor phlogopite with Fe oxides and Fe sulphides (Section 4.4.5). Low SiO_2 and Al_2O_3 contents within these rocks are believed to prevent the occurrence of epidote, which is characteristic of the low-grade calcareous litharenites and impure calcirudites. The presence of K_2O has allowed phlogopite to form. However, if K_2O was absent an amphibole is likely to have formed in its place. Near the contact of the Inlet Monzonite, forsterite marbles have resulted from the contact metamorphism of this rock type. Their low Al_2O_3 content is exemplified by the absence of garnet. These marbles also lack diopside, which reflects their low SiO_2 content, and contain no obvious K-bearing phase. The formation of forsterite marbles in contrast to calcareous rocks containing assemblages of garnet, clinopyroxene and wollastonite was discussed by Harker (1974, p.87) in reference to their differences in Al_2O_3 content.

The calcareous litharenites become virtually opaque-free at the garnet isograd, with Fe entering the garnet (andradite component) and clinopyroxene (hedenbergite component) in preference to forming opaque oxides and sulphides of Fe. However, in the stylolitic limestones these opaques occur throughout the aureole, as garnet and clinopyroxene are unable to form. Although the Al_2O_3 content in the stylolitic limestones is significantly lower than in the other rock types studied, the presence

of some Al_2O_3 is characteristic, and contrasts it with siliceous dolomites, whose bulk-rock composition can be approximated by the CaO-MgO-SiO_2-H_2O system (Kerrick, 1974). The Al_2O_3 component of the stylolitic limestones occurs within the phlogopite at low grade (or in amphibole if K_2O is absent), while at higher grade, with the formation of forsterite, Al has gone to form spinel. The compositional and mineralogical differences between the stylolitic limestones and the other impure calcareous rocks described in this study are believed to reflect the low quartzo-feldspathic content of the original stylolitic limestone. That is, the other impure calcareous rocks represent mixtures of calcareous, psammitic, pelitic, and volcanic material, with quartz and feldspar being dominant phases, whereas the stylolitic limestones appear to represent calcite-rich rocks that originally contained only minor clay impurities.

4.7 METAMORPHIC CONDITIONS

4.7.1 Discussion of T-X_{CO_2} Diagrams

Experimental data pertinent to the assemblages of this study have been collated on isobaric T-X_{CO_2} diagrams for 1 and 2 kb (pressures typical of contact metamorphism), in Figs. 4-7 and 4-8 respectively. The curves in Figs. 4-7 and 4-8 have been modified, where feasible, to allow for solid solution in the phases. This has been based on mineral compositions within the calcareous litharenites (Section 4.5), and the appropriate mineral compositions (e.g. the $Al/Al+Fe^{3+}$ ratio or grossular content of garnet, or the $Mg/Mg+Fe^{2+}$ ratio of clinopyroxene) are designated on the curves. The modifications are achieved by equating, at a particular temperature and pressure, the equilibrium constants for a given reaction, calculated for different compositions within the reactants and products. That is, the equilibrium constant for a reaction whose position in P-T-X_{CO_2} space is known for certain compositions in the phases (typically end-member compositions) is equated to the equilibrium constant for the same reaction calculated for phase compositions for which the reaction's position in P-T-X_{CO_2} space is unknown. In this way X_{CO_2} values for the reaction involving the latter phase compositions can be calculated. The thermodynamic basis of equating equilibrium constants is briefly outlined here, and further discussion of the shifting of curves on the T-X_{CO_2} diagram is given below.

The free energy of a reaction at pressure P_1 and temperature T_1 can be expressed as

$$\left(\Delta G_r\right)_{T_1}^{P_1} = \left(\Delta G_r^o\right)_{T_1}^{P_1} + RT_1 \ell n\left(K\right)_{T_1}^{P_1} \qquad A$$

where ΔG_r^o = standard state free energy change of a reaction

R = gas constant

T = temperature

K = equilibrium constant (a ratio of the activities of products and reactants in the reaction, Wood and Frazer, 1976, p.66).

At equilibrium this becomes

$$\left(\Delta G_r^o\right)_{T_1}^{P_1} = -RT_1 \ell n\left(K\right)_{T_1}^{P_1} \qquad B$$

ΔG_r^o at a particular temperature and pressure of interest can also be expressed in terms of thermochemical data:

$$\left(\Delta G_r^o\right)_{T_1}^{P_1} = \Delta H^o_{T_1,1\text{ bar}} - T_1 \Delta S^o_{T_1} + \left(P_1 - 1\right) \Delta V_s^o \qquad C$$

where $\Delta H^o_{T_1,1\text{ bar}}$ = standard state enthalpy change for the reaction at T_1, 1 bar;

$\Delta S^o_{T_1}$ = standard state entropy change for the reaction T_1;

ΔV_s^o = standard state volume change in the solids for the reaction at T_1, 1 bar.

Combining equations B and C shows that for a constant temperature and pressure ℓn K will be constant, and hence equilibrium constants (for different activities in the phases) can be equated. Ghent and De Vries (1972, pp.630-631) stated this relationship in terms of the Van't Hoff equation:

$$\frac{d\ \ell n\ K}{d\ T} = \frac{\Delta H^o}{RT^2} \quad ,$$

which is derived for constant pressure at 1 bar (standard state) (Garrels and Christ, 1965, p.349).

Slaughter *et al.* (1976) presented a computer program (MULTIPTX) for extrapolating from starting points of equilibrium to new points in P-T-X_{CO_2} space. This program is based on equations A and B, describing

a starting point P_1T_1 and equation D for locating a new point P_2T_2:

$$\left(\Delta G_r\right)_{T_2}^{P_2} = \left(\Delta G_r^o\right)_{T_1}^{P_1} - \int_{T_1}^{T_2} \Delta S_s^o \, dT + \int_{P_1}^{P_2} \Delta V_s^o \, dP + \left(G_{H_2O}\right)_{T_2}^{P_2} - \left(G_{H_2O}\right)_{T_1}^{P_1}$$

$$+ \left(G_{CO_2}\right)_{T_2}^{P_2} - \left(G_{CO_2}\right)_{T_1}^{P_1} + R\,T_2\,\ell n\,K_2 \qquad D$$

where ΔS_s^o = standard state entropy change of solids in the reaction

ΔV_s^o = standard state volume change of solids in the reaction

G_{H_2O} = free energy of pure H_2O

G_{CO_2} = free energy of pure CO_2

From equations B and D it is apparent that for new equilibrium points derived at the same pressure and temperature (with different activites in the phases), equation D becomes $RT\,\ell n\,K_1 = RT\,\ell n\,K_2$, allowing K_1 to be equated to K_2. This derivation is fundamentally identical to that described above.

Activities, used in calculating equilibrium constants, are calculated from mole fractions on the basis of the cationic substitution model, as used, for example, by Ghent and De Vries (1972), Wood and Fraser (1976), Kerrick (1977), Skippen and Carmichael (1977), and Erdmer (1981). In this work, equilibrium constants for reactions containing solid-solution phases are equated to those for reactions involving solids of pure end-member compositions (the activity of pure solids at the pressure and temperature of interest is taken as unity; Wood and Fraser 1976, p.56). As the $T\text{-}X_{CO_2}$ locations of the latter curves are commonly known for different isobaric sections, the required shift in X_{CO_2} to allow for the change in activities of the phases can be calculated by equating equilibrium constants. Several calculations of this type at different temperatures will derive a modified curve for specific compositions in the phases. A straightforward example of shifting curves in this manner is presented by Kerrick *et al.* (1973). However, it should be noted that these authors have considered a molecular solution model to derive activities, rather than the cationic model preferred here and by most recent authors.

As insufficient thermodynamic data are available on the solid phases, calculations have been carried out on the basis of ideal mixing in the solids (in agreement with Kerrick, 1974,1977). However, in accordance with Kerrick (1977), non-ideal mixing in the volatile phases has been corrected for by using the fugacity coefficients (converted to activity coefficients (γ)) of Ryzhenko and Malinin (1971) (i.e. activity (a) = activity coefficient (γ).mole fraction (X)). Manual shifts of the curves in Figs. 4-7 and 4-8 agree accurately with those computed by Kerrick (1977, Fig. 2), except that Kerrick, in shifting the curve representing the reaction

$$2 \text{ Zoisite} + CO_2 \rightarrow 3 \text{ Anorthite} + \text{Calcite} + H_2O,$$

to allow for solid solution in the epidote, ignored (the present author believes incorrectly) the reaction coefficients in his calculations. Therefore, Kerrick's modified curves for this reaction lie at lower X_{CO_2} values than those shown in Fig. 4-8.

A worked example of calculations used to shift curve 1 (Fig. 4-7) to allow for solid solution in the garnet and plagioclase is shown in Appendix Two.

4.7.2 Calcareous Litharenites

This section relates the observed paragenesis and proposed sequence of reactions in the calcareous litharenites to the prograde sequence of experimentally determined curves shown in Figs. 4-7 and 4-8. Buffering of the pore fluid is initially considered, before discussing the X_{CO_2} values and temperature changes associated with progressive metamorphism within the northern aureole of the Inlet Monzonite.

Buffering of the Pore Fluid

Kerrick (1974) discussed the differences between local and external control of fluid composition (closed and open systems respectively), and noted that in a closed system, buffering of the pore fluid composition is to be expected. Greenwood (1975) has discussed the buffering of pore fluids by metamorphic reactions, and several authors, including Trommsdorf (1972), Suzuki (1977) and Rice (1977), have described natural examples where such buffering appears to have taken place. Most natural

Figure 4-7: T-X_{CO_2} diagram at 1 Kb for some equilibria in the system K_2O-CaO(Na_2O)-MgO(FeO)-Al_2O_3(Fe_2O_3)-SiO_2-CO_2-H_2O.

Source of equilibria are:

1. Kerrick (1970)
2. Newton (1966)
3. Greenwood (1967)
4. Based on the topology of Kerrick (1974).
5. Same as 4.
6. Extrapolated from Kerrick's (1977) data at 2 Kb, based on data for the reaction at different pressures from Storre and Nitsch (1972).
7. Extrapolated from Hoschek's (1980) data at 5 Kb, based on data for associated reactions at different pressures from Slaughter *et al.* (1975).
8. Same as 7.
9. Rice (1977).
10. Rice (1977).

Curves 1',2',2^{IV},4',4'',4''',5A,6''',8A,10A have been derived by modification of the appropriate curve for solid solution in the phases. Mineral compositions have been recorded from the calcareous litharenites. The method of modification is described in the text, and a worked example is presented in Appendix II. Values on the modified curves refer to:

the anorthite content of plagioclase (e.g. An 80);
the grossular content ($Al/Al+Fe^{3+}$ ratio) of garnet (e.g. Gr 40);
the zoisite content ($Al/Al+Fe^{3+}$ ratio) of epidote (e.g. Zo 40)†;
the Mg/Mg+Fe ratio of diopside, tremolite, and chlorite (e.g. Di 68, Tr 64, Chl 31).

Estimated limits for X_{CO_2} in the pore fluid of the calcareous litharenites are shown as a lightly stippled region. These limits are discussed in the text. Reactions relevant to the contact metamorphsim of calcareous litharenites at the Horse Arm Creek locality are shown as darker lines (within the stippled region).

An = anorthite, Bi = biotite, Cal = calcite, Chl = chlorite, Di = diopside, Gr = grossular, K-f = K-feldspar, Musc = muscovite, Phl = phlogopite, Tr = tremolite, Qtz = Quartz, Woll = wollastonite, Zo = zoisite.

†The activity of zoisite (a_{Zo}), used in shifting curves for Fe substitution in the epidotes, is equal to the fractional occupancy of Al in the M3 site (X^{M3}_{Al}) (Kerrick, 1977). For example an epidote with an $Al/Al+Fe^{3+}$ ratio = 0.75 (i.e. Zo 75) has an activity of zoisite equal to 0.25.

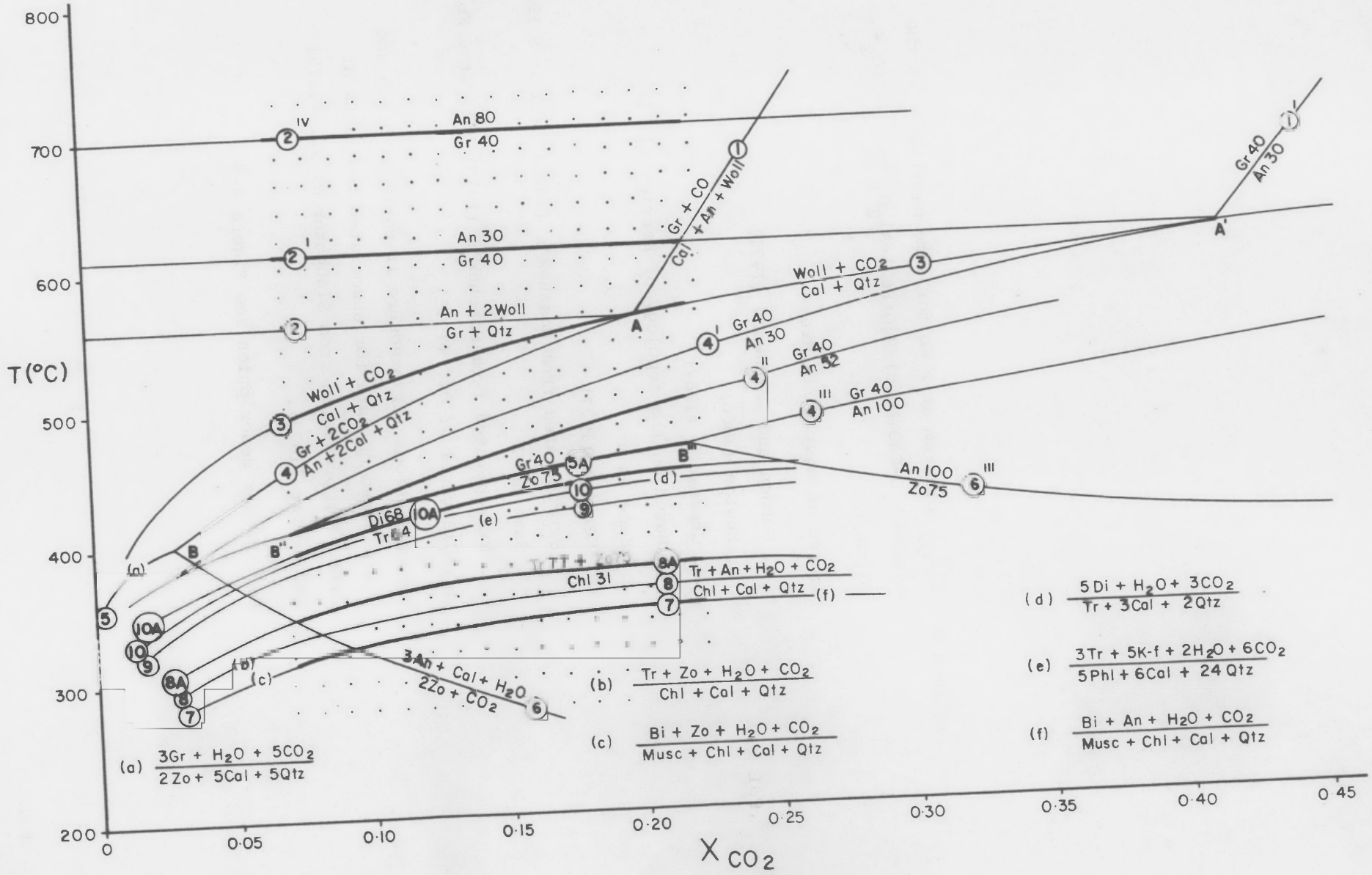
T(°C)
800
700
600
500
400
300
200
0
0·05
0·10
0·15
0·20
0·25
0·30
0·35
0·40
0·45
X CO2
An 80
Gr 40
An 30
Gr 40
An + 2Woll
Gr + Qtz
Woll + CO2
Cal + Qtz
Gr + 2CO2
An + 2Cal + Qtz
Gr + CO
Cal + An + Woll
Gr 40
An 30
Gr 40
An 52
Gr 40
An 100
An 100
Zo75
Gr 40
Zo75
Di68
Tr 4
Chl 31
3An + Cal + H2O
2Zo + CO2
Tr + An + H2O + CO2
Chl + Cal + Qtz
(a) 3Gr + H2O + 5CO2 / 2Zo + 5Cal + 5Qtz
(b) Tr + Zo + H2O + CO2 / Chl + Cal + Qtz
(c) Bi + Zo + H2O + CO2 / Musc + Chl + Cal + Qtz
(d) 5Di + H2O + 3CO2 / Tr + 3Cal + 2Qtz
(e) 3Tr + 5K-f + 2H2O + 6CO2 / 5Phl + 6Cal + 24Qtz
(f) Bi + An + H2O + CO2 / Musc + Chl + Cal + Qtz

Figure 4-8: $T\text{-}X_{CO_2}$ diagram at 2 Kb for some equilibria in the system K_2O-CaO(Na_2O)-MgO(FeO)-Al_2O_3(Fe_2O_3)-SiO_2-CO_2-H_2O.

Source of equilibria are:

1. Gordon and Greenwood (1971)
2. Newton (1966)
3. Greenwood (1967)
4. Based on the topology of Kerrick (1974)
5. Same as 4
6. Kerrick (1977)
7. Extrapolated from Hoschek's (1980) data at 5 Kb
8. Same as 7
9. Extrapolated from Hoschek's (1973) data at 6 Kb
10. Slaughter *et al.* (1975)

Extrapolations for pressure in equilibria 7,8 and 9 are based on data for associated reactions at different pressures from Slaughter *et al.* (1975) and Hewitt (1973).

For further description see Figure 4-7.

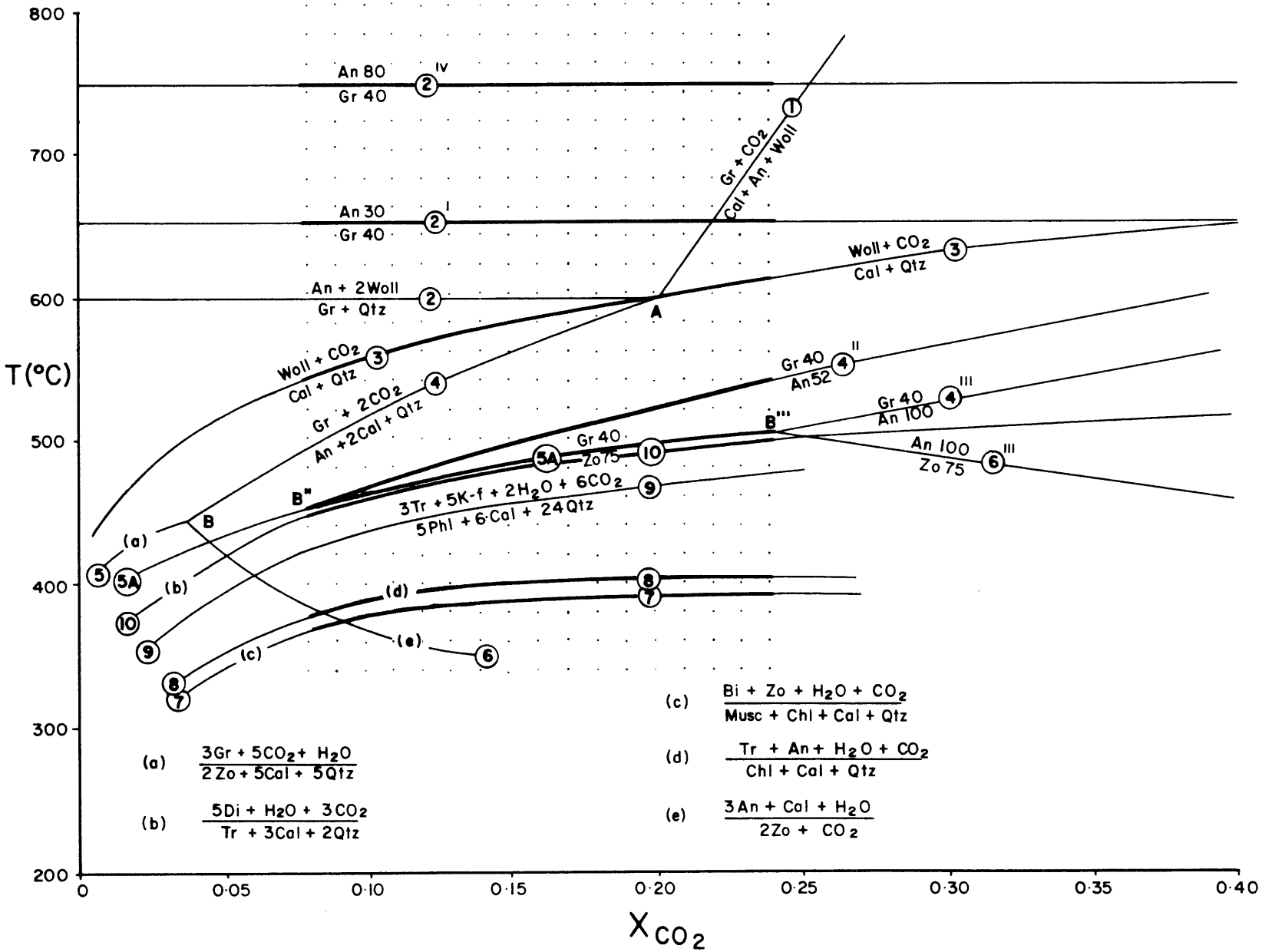
800
700
600
500
400
300
200
T(°C)
0
0·05
0·10
0·15
0·20
0·25
0·30
0·35
0·40
X_{CO_2}
An 80
Gr 40
IV
An 30
Gr 40
I
An + 2Woll
Gr + Qtz
Gr + CO2
Cal + An + Woll
Woll + CO2
Cal + Qtz
Woll + CO2
Cal + Qtz
Gr + 2CO2
An + 2Cal + Qtz
Gr 40
An52
II
Gr 40
An 100
III
An 100
Zo 75
III
Gr 40
Zo 75
3Tr + 5K-f + 2H2O + 6CO2
5Phl + 6Cal + 24Qtz
A
B
B''
B'''
(a)
(b)
(c)
(d)
(e)
(a) 3Gr + 5CO2 + H2O / 2Zo + 5Cal + 5Qtz
(b) 5Di + H2O + 3CO2 / Tr + 3Cal + 2Qtz
(c) Bi + Zo + H2O + CO2 / Musc + Chl + Cal + Qtz
(d) Tr + An + H2O + CO2 / Chl + Cal + Qtz
(e) 3An + Cal + H2O / 2Zo + CO2

examples have been described within siliceous dolomites. If buffering operates, isobaric univariant assemblages should be common, and the most conspicuous changes in mineral assemblages (zone boundaries) should occur at isobaric invariant points (Greenwood, 1975). However, in this study, sharp zone boundaries appear to be defined by isobaric univariant reactions, for the general reactions described in Section 4.6 can be represented on T-X_{CO_2} diagrams as univariant curves (outlined below with reference to Figs. 4-7 and 4-8), and assemblages of reactants and products defined by these reactions (isobaric univariant assemblages) are rare. Therefore, reactions within these rocks do not seem to buffer the fluid composition.

This feature could be related to a small extent of buffering occurring at the zone boundaries (small amounts of buffering would be difficult to detect) or external control of the fluid composition, or both. The low-grade reactions (those at temperatures below the garnet isograd) of Section 4.6 would not be expected to greatly buffer the composition of the fluid phase, because both CO_2 and H_2O are evolved. Also buffering at the biotite isograd (decreasing X_{CO_2}) would have the opposite effect to buffering at the clinopyroxene isograd (increasing X_{CO_2}), and the overall change in fluid composition would be small. However, in the higher-grade reactions (the garnet isograd and above) the X_{CO_2} values should increase, because CO_2 is the major vapour phase released. Therefore, the lack of buffering at these higher-grade boundaries implies that the fluid composition is being externally controlled with regard to the reactions taking place. However, in inhomogeneous rocks such as those studied here, this does not necessarily imply that the fluid composition is being externally controlled. Although the higher-grade reactions involving the breakdown of carbonate are readily detectable, the proportion of the rock affected by such reactions can be small compared to its total volume. Hence, the local buffering associated with the reactions is probably insufficient to effectively control the fluid composition as a whole. Similarly, dehydration reactions associated with the non-calcareous component of the rocks would help maintain a high water content in the fluid phase.

Therefore, because buffering is unlikely to have greatly affected the fluid composition, the path of metamorphism can be considered to occur within a small range of X_{CO_2} values. This is in contrast to carbonate-

rich rocks, such as siliceous dolomites, where large amounts of CO_2 are derived from the breakdown of carbonates throughout the rock. In such rocks, buffering of the fluid phase to higher concentrations of CO_2 would be expected, unless a major influx of water from surrounding rocks took place during metamorphism.

X_{CO_2} in the Fluid Phase

Epidote Zo 75 is stable in the outer part of the aureole until the garnet isograd where it is replaced by garnet Gr 40 (reaction 4-VI, Section 4.6.2). This is represented by the general equation

2 Epidote (Zo 75) + Calcite + Quartz → 3 Garnet (Gr 40) + 5 CO_2 + H_2O

and represented by curve 5A in Figs. 4-7 and 4-8. Also, there is no evidence of epidote breaking down to cause an increase in An content of the plagioclase. Therefore, X_{CO_2} must lie to the low-X_{CO_2} side of curve 6''' (Figs. 4-7 and 4-8), and consequently, to the low-X_{CO_2} side of B''' . This requires X_{CO_2} to be less than 0.22 for 1 kb and 0.24 for 2 kb.

In addition, the formation of garnet has been also attributed to reaction 4-VII (Section 4.6.2), which in general form is

Plagioclase (An 52) + 2 Calcite + 3 Quartz → Garnet (Gr 40) + 2 CO_2

with An 52 being the average composition of the relict plagioclase. This reaction is represented by curve 4' in Figs. 4-7 and 4-8. For both curves 5A and 4' to be intersected with increasing temperature, without extensive buffering of the pore fluid (discussed above), X_{CO_2} values must lie in the range 0.06 → 0.22 at 1 kb, or 0.08 → 0.24 at 2 kb. Because of the apparent lack of buffering of the pore fluid during metamorphism, these constraints on X_{CO_2} are broadly applicable to the metamorphism of the calcareous litharenites throughout the aureole, and are shown as stippled regions in Figs. 4-7 and 4-8. It is emphasised though, that the actual path of metamorphism is believed to occur within a small range of X_{CO_2}, but the position of this path can be only broadly constrained within the limits outlined above.

Biotite Zone

The incoming of biotite is associated with the breakdown of K-feldspar + calcite + chlorite (reaction 4-I, Section 4.6.2). No experimental data

are available on such a reaction. Therefore, it is assumed here to occur at temperatures roughly similar to those represented by curve 7, involving muscovite rather than K-feldspar. On the high-X_{CO_2} side of the Zo → An + Cal stability curve (curve 6, Figs. 4-7 and 4-8), anorthite is stable relative to zoisite on curve 7. Hence, for Al end members this would require anorthite + biotite to be the stable products of reaction 7 for a major part of the proposed range of X_{CO_2} values. However, epidote within the biotite zone is Zo 75, and the stability of epidote Zo 75 relative to anorthite is governed by curve 6''' (Figs. 4-7 and 4-8). Consequently, in the proposed range of X_{CO_2} values epidote Zo 75 + biotite is stable, in accord with the petrography of the biotite zone. Relict plagioclase (An 52) is present within the biotite zone. However, the stability of epidote is not determined relative to An 52, because the relict plagioclase is not involved in the formation of epidote (via reaction 7), and the epidote and relict plagioclase are apparently not in chemical equilibrium.

Based on reaction 7, temperatures for the incoming of biotite at 1 kb are broadly estimated at between 300 and 350°C (for the proposed range of X_{CO_2} values) (Fig. 4-7) and 330 → 390°C at 2 kb (Fig. 4-8).

Clinopyroxene Zone

Evidence exists within the clinopyroxene zone for the reactions

chlorite + calcite + quartz → amphibole + epidote

tremolite + calcite + quartz → clinopyroxene

(Section 4.4.2). Balanced equations for these mineralogical changes have been proposed in Section 4.6.2; i.e. 4-IV(A or B) and 4-V. Although the amphibole in these rocks is strictly magnesio-hornblende (after Leake, 1978), these reactions can be considered as equivalent to curves 8 and 10 in Figs. 4-7 and 4-8 (8A and 10A, allowing for the appropriate solid solution). Therefore, temperatures above these curves are suggested for the clinopyroxene zone, with 10 (10A) possibly marking the clinopyroxene isograd.

However, there is no evidence of an amphibole + K-feldspar zone, expected between curves 9 and 10 (Figs. 4-7 and 4-8), even though biotite is a prominent phase below the clinopyroxene isograd. The absence of an amphibole + K-feldspar zone is believed to be the result of Fe

substitution in the phases. Thompson (1975b, Fig. 8, reproduced here as Fig. 4-6) has shown, on a T-X(Fe-Mg) diagram, that with the addition of Fe in the reacting phases, curves 9 and 10 (Fig. 4-7) intersect to become metastable with respect to the clinopyroxene + K-feldspar-forming reaction:

Biotite + 3 Calcite + 6 Quartz → 3 Clinopyroxene + K-feldspar + H_2O + 3 CO_2.

This intersection is schematically shown as point X on the T-X_{CO_2} diagram in Fig. 4-9, based on Thompson (1975b). The clinopyroxene + K-feldspar-forming reaction is represented as curve 11 in Fig. 4-9. Curves 12 and 13, which also occur at this intersection, are discussed by Thompson (1975b). The arrowed path in Fig. 4-9 represents a possible path of progressive metamorphism for host-rock compositions in the calcareous litharenites able to form biotite at lower temperatures. Reaction 13 will not occur, because no K-feldspar remains after the formation of biotite, and the clinopyroxene isograd is designated by reaction 11 (equivalent to reaction 4-III, Section 4.6.2). In K_2O-poor domains of the rocks (lacking biotite at lower grade) metamorphism would proceed via reactions 8 and 10. Hence, there is evidence of these reactions only in restricted parts of the rocks within the clinopyroxene zone (noted above).

Temperatures for the clinopyroxene isograd can be estimated by assuming reaction 11 to occur at temperatures between those of curves 9 and 10. At 1 kb (Fig. 4-7), this broadly suggests a temperature range for the clinopyroxene isograd of 380 → 430°C, depending on X_{CO_2}, and at 2 kb (Fig. 4-8) a range of 430 → 490°C.

Garnet Zone

The formation of garnet has been attributed to two reactions (Section 4.6.2: reactions 4-VI and 4-VII), as described in the above discussion on X_{CO_2} of the fluid phase. These reactions are represented in Figs. 4-7 and 4-8 as curves 5A and 4'. Based on curve 5A (the lower-temperature curve), the incoming of garnet at 1 kb can occur between 410 and 460°C in the proposed X_{CO_2} range, and 2 kb, 450 → 510°C.

The topology of Fig. 4-7 is compatible with the sequence of zones recognised in this study because garnet has not formed, via curve 5, until temperatures above those of curve 10A were achieved. However, in

Figure 4-9: Schematic representation of the intersection of curves 9 and 10 (Figure 4-7), as a result of Fe substitution in the phases (the curves are designated 9' and 10'). This figure is based on data from Thompson (1975b). The reactions represented by the curves are discussed by Thompson (1975b). X is the invariant point defined by the intersection of these curves. X' represents a schematic intersection of the same curves with higher Fe substitution in the phases. The arrowed path shows a possible path of progressive metamorphism for host-rock compositions in the calcareous litharenites able to form biotite at lower temperature.

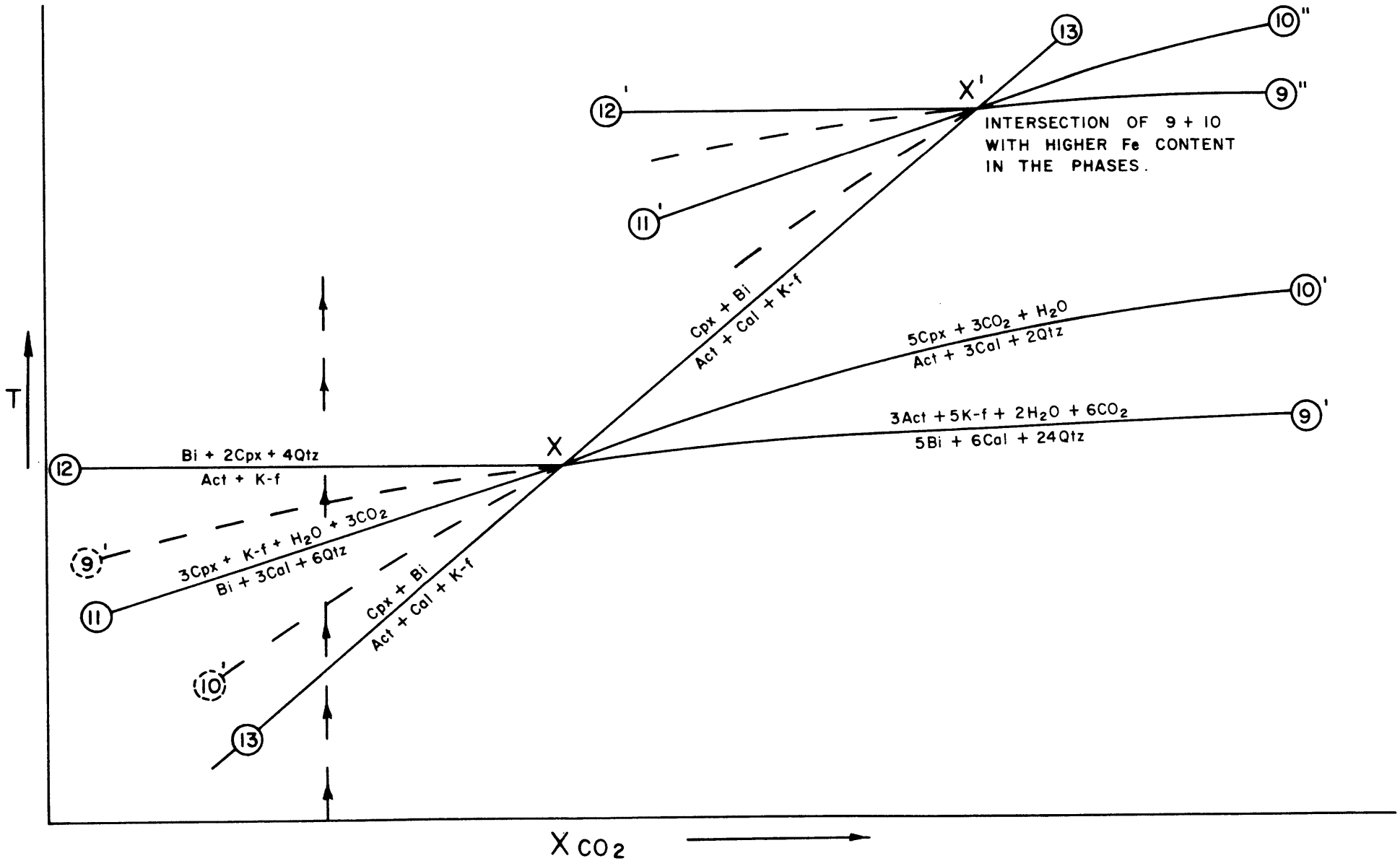
T
X CO2
X
X'
12
11
10
9
13
Bi + 2Cpx + 4Qtz
Act + K-f
3Cpx + K-f + H2O + 3CO2
Bi + 3Cal + 6Qtz
Cpx + Bi
Act + Cal + K-f
5Cpx + 3CO2 + H2O
Act + 3Cal + 2Qtz
3Act + 5K-f + 2H2O + 6CO2
5Bi + 6Cal + 24Qtz
INTERSECTION OF 9 + 10
WITH HIGHER Fe CONTENT
IN THE PHASES.

Fig. 4-8, curves 5 and 10 are closely related in temperature, and indeed, if curve 10 is corrected for solid solution (as in Fig. 4-7), garnet could be stable below curve 10. This is inconsistent with the petrography of the calcareous litharenites. Allowances must be made for the uncertainties in the curves, but this does suggest that pressures below 2 kb are more likely, and Fig. 4-7 at 1 kb appears to give a better representation of the path of metamorphism.

Wollastonite-bearing Zones

The incoming of wollastonite requires temperatures above those of curve 3 (Figs. 4-7 and 4-8). For 1 kb, temperatures for the wollastonite isograd range from 490 → 560°C, depending on X_{CO_2}. At 3 kb, these temperatures are raised by 40°C. With a further increase in temperature wollastonite + plagioclase An 30 becomes stable in preference to quartz + garnet Gr 40, defining the wollastonite + plagioclase zone. This boundary is represented in Figs. 4-7 and 4-8 by curve 2, and is independent of X_{CO_2}. At 1 kb this boundary occurs at 610°C, whereas at 2 kb it occurs at 650°C. Plagioclase with higher An contents are apparently stable with wollastonite in the higher-grade parts of the wollastonite + plagioclase zone. Near the contact, plagioclase An 80 has been recorded with wollastonite (Section 4.5.6), and therefore curve 2^{IV} (An 80, Gr 40) can be used to define likely contact temperatures. For 1 kb, contact temperatures of around 700°C are suggested, whereas at 2 kb temperatures are nearer 750°C.

Conclusions

From Figs. 4-7 and 4-8 it is apparent that reaction temperatures are dependent on pressure and, in the case of reactions involving a volatile phase, on X_{CO_2}. As neither pressure nor X_{CO_2} can be determined precisely, and because of the uncertainties in representing complex natural reactions by the simple modified curves of Figs. 4-7 and 4-8, exact temperatures for the reactions cannot be given. However, allowing for these limitations, broad estimates of the metamorphic conditions can be made. From the above discussion, pressures below 2 kb, and X_{CO_2} values between 0.06 and 0.22 are applicable to the sequence of metamorphic zones identified within the calcareous litharenites. Such conditions imply temperatures ranging from around 350°C at the outer edge of the aureole

of the Inlet Monzonite up to 700 → 750°C at the contact. Similarly, the zone boundaries are believed to roughly correlate with temperatures given for the appropriate reactions in the above discussion.

4.7.3 Impure Calcirudites

The sequence of metamorphic zones in these coarse-grained rocks is the same as that recognised in the calcareous litharenites. Therefore a similar path of metamorphism is expected for the matrix assemblages in these rocks as that outlined in Section 4.7.2.

The metamorphic zones in the Moonbi aureole have been defined in the South Kootingal locality using impure calcirudites. Although zone widths depend on the characteristics of the pluton (Section 1.6.2), the South Kootingal aureole appears to have a garnet zone thinner than that defined by the calcareous litharenites in the northern aureole of the Inlet Monzonite (Section 4.4.3). The uncertainty in locating zone boundaries at the South Kootingal locality may account for this discrepancy. Alternatively, this disparity may be caused by compositional differences in the rocks. Garnets within the impure calcirudites typically have higher $Al/Al+Fe^{3+}$ ratios than garnets in the calcareous litharenites (Section 4.5.3). From Fig. 4-7, this would require higher temperatures for garnet formation in the impure calcirudites, consistent with the occurrence of a thinner garnet zone at the South Kootingal locality. The clinopyroxene zone at South Kootingal is also significantly wider than that developed in the calcareous litharenites north of the Inlet Monzonite. This could simply be a consequence of the thinner garnet zone. However, the tendency toward higher $Mg/Mg+Fe^{2+}$ ratios in the clinopyroxenes of the impure calcirudites compared to those in the calcareous litharenites (Section 4.5.4), would also tend to form clinopyroxenes at lower temperatures at the South Kootingal locality (Figs. 4-7 and 4-9).

4.7.4 Impure Biomicrites

Two zone-boundary reactions have been recognised within the impure biomicrites (Section 4.6.3):

1) Biotite + 3 Calcite + 6 Quartz → 3 Clinopyroxene + K-feldspar + H_2O + 3 CO_2

2) Calcite + Quartz → Wollastonite + CO_2.

However, garnet has not formed at temperatures between these reactions, as described in both the calcareous litharenites and the impure calcirudites. Metamorphism therefore appears to have taken place at higher X_{CO_2} values than those suggested in Fig. 4-7, with X_{CO_2} values lying to the CO_2-rich side of invariant point A. How high the X_{CO_2} values need to be to prevent formation of garnet depends on the mineral chemistry, for this affects the location of point A (to A' etc). This is consistent with the more-calcareous nature of the impure biomicrites relative to the calcareous litharenites and impure calcirudites.

The clinopyroxene and wollastonite isograds occur closer to the pluton contacts in the impure biomicrites than in the other impure calcareous rocks. This is consistent with metamorphism at higher X_{CO_2} values, because reactions corresponding to these isograds take place at higher temperatures with increasing X_{CO_2} (Fig. 4-7), at least until X_{CO_2} values of 0.5 are exceeded.

In the impure biomicrites, wollastonite, calcite and quartz occur in apparent equilibrium in the vicinity of the wollastonite isograd. This implies that the pore fluid has been buffered at this boundary, stabilising this assemblage over a temperature interval. Hence, CO_2 derived from the formation of wollastonite has been sufficient to cause a significant shift in X_{CO_2} of the pore fluid. This is in contrast to the calcareous litharenites, where buffering of the pore fluid does not appear to have occurred (Section 4.7.2), and again this reflects the more-calcareous composition of the impure biomicrites.

4.8 SUMMARY

Several impure calcareous rock types have been studied within the contact aureoles of the Inlet Monzonite and the Moonbi Adamellite, at three separate localities in the Tamworth Group. These rocks predominantly consist of inhomogeneous mixtures of clastic calcareous and non-calcareous material. They vary in grainsize (arenaceous to rudaceous) and composition, both within and between units. The bulk-rock composition for most rocks in this study can be approximated by the K_2O-CaO-MgO-Al_2O_3-SiO_2-CO_2-H_2O system.

Outside the aureole, the sediments have been affected by very

low-grade regional metamorphism. Within the aureole, five zones based on the recognition of metamorphic assemblages, usually delineated by the appearance of a new phase, have been defined within the calcareous litharenites:

I) Biotite Zone
II) Clinopyroxene Zone
III) Garnet Zone
IV) Wollastonite Zone
V) Wollastonite + Plagioclase Zone

The same sequence of zones has been recognised in the matrix material of coarser-grained impure calcirudites. Impure biomicrites and a highly calcareous unit of stylolitic limestone are described separately.

Chemical variations occurring in the phases are mainly related to variations in host-rock chemistry. No systematic trends in mineral chemistry can be related to increasing grade. However, metamorphic plagioclase developed within the higher-grade zones is characteristically more albitic than relict plagioclase in the same rock.

Balanced equations for the reactions representing the mineralogical changes within the calcareous litharenites have been derived from probe data. Experimentally determined curves appropriate to the proposed reactions have been represented on isobaric T-X_{CO_2} diagrams for 1 and 2 kb. Where possible, these reactions have been modified for solid solution within the phases. This has been carried out by equating equilibrium constants at the same temperature and pressure, but for varying compositions (activities) in the phases.

The metamorphic zones within the impure calcareous rocks of this study are characterised by sharp zone boundaries. On an isobaric T-X_{CO_2} diagram, these zone boundaries are represented by univariant curves (which separate divariant fields, denoting the metamorphic zones), and univariant assemblages defined by these curves are very rarely found. That is, reactants and products involved in the boundary reactions do not appear to coexist over significant temperature intervals (the wollastonite isograd in the impure biomicrites is an exception). This implies two important features about the nature of these reactions. One, the reactions are discontinuous, and two, they do not appear to buffer the pore fluid

composition. The discontinuous nature of the reactions is due to the availability of additional phases (especially Fe oxides), which balance the reactions without requiring compositional adjustment of the phases. The lack of buffering of the pore fluid is believed to be related to the inhomogeneous nature of the rocks studied, rather than any external control of the fluid composition. Local buffering associated with reactions described in this chapter, where there is a significant imbalance in the moles of H_2O and CO_2 evolved, is unlikely to affect a sufficiently large proportion of the rock to effectively control the fluid composition.

Broad estimates have been determined for the contact metamorphic conditions occurring within the calcareous litharenites of the northern aureole of the Inlet Monzonite. These conditions have been approximated at pressures of below 2 kb, X_{CO_2} in the fluid phase between 0.06 and 0.22, and temperatures ranging from around 350^{o}C at the outer edge of the aureole ($\simeq$ 2 km from the contact) up to 700-750^{o}C at the contact.